The DOI for this manuscript is doi: 10.1175/JCLI-D-18-0474.1

Volkov, D., M. Baringer, D. Smeed, W. Johns, and F. Landerer, 2018: Teleconnection between the Atlantic Meridional Overturning Circulation and sea level in the Mediterranean Sea. J. Climate. doi:10.1175/JCLI-D-18-0474.1, in press.

Teleconnection between the Atlantic Meridional Overturning Circulation and sea level in the Mediterranean Sea

Denis L. Volkov[1,2], Molly Baringer[2], David Smeed[3], William Johns[4], Felix W. Landerer[5]

[1]Cooperative Institute for Marine and Atmospheric Studies, University of Miami, Miami, Florida, USA

[2]National Oceanic and Atmospheric Administration, Atlantic Oceanographic and Meteorological Laboratory, Miami, Florida, USA

[3]National Oceanography Centre, Southampton, United Kingdom

[4]Rosenstiel School of Marine and Atmospheric Science, University of Miami, Miami, Florida, USA

[5]Jet Propulsion Laboratory, California Institute of Technology, Pasadena, USA

Corresponding author contact information:

Dr. Denis L. Volkov
CIMAS / University of Miami
NOAA - AOML / PhOD
4301 Rickenbacker Causeway
Miami, FL 33149, USA
Tel: +1-(305)-361-4344
Email: denis.volkov@noaa.gov

Submitted to Journal of Climate
July 23, 2018
Revised: October 11, 2018

Abstract

The Mediterranean Sea can be viewed as a "barometer" of the North Atlantic Ocean, because its sea level responds to oceanic-gyre-scale changes in atmospheric pressure and wind forcing, related to the North Atlantic Oscillation (NAO). The climate of the North Atlantic is influenced by the Atlantic Meridional Overturning Circulation (AMOC) as it transports heat from the South Atlantic towards the Subpolar North Atlantic. This study reports on a teleconnection between the AMOC transport measured at 26.5°N and the Mediterranean Sea level during 2004-2017: a reduced/increased AMOC transport is associated with a higher/lower sea level in the Mediterranean. Processes responsible for this teleconnection are analyzed in detail using available satellite and in situ observations, and an atmospheric reanalysis. Firstly, it is shown that on monthly to interannual time scales the AMOC and sea level are both driven by similar NAO-like atmospheric circulation patterns. During a positive/negative NAO state, stronger/weaker trade winds (i) drive northward/southward anomalies of Ekman transport across 26.5°N that directly affect the AMOC, and (ii) are associated with westward/eastward winds over the Strait of Gibraltar that force water to flow out/in the Mediterranean Sea and thus change its average sea level. Secondly, it is demonstrated that interannual changes in the AMOC transport can lead to thermosteric sea level anomalies near the North Atlantic eastern boundary. These anomalies can (i) reach the Strait of Gibraltar and cause sea level changes in the Mediterranean Sea, and (ii) represent a mechanism for negative feedback on the AMOC.

1. Introduction

The Atlantic Ocean is unique for the Earth's climate system as it is the only ocean where net heat is transported from the Southern Hemisphere across the equator towards the northern subpolar gyre. As the upper warm waters flow northward, they lose heat to the atmosphere, become cooler and denser, and form deep water in the Labrador and Nordic Seas that then return southward comprising the Atlantic Meridional Overturning Circulation (AMOC) (Figure 1). The northward heat transport reaches a maximum of 1.3 PW near 24-26°N (Hall and Bryden 1982; Trenberth and Caron 2001), with a balanced volume transport between the northward flow of warm Gulf Stream waters and wind-driven surface flow (Ekman transport) and the southward flow of cooler thermocline and cold North Atlantic Deep Water. Much of the heat transferred from the ocean to the atmosphere at mid-latitudes of the North Atlantic is carried eastward by westerly winds and contributes to the temperate climate of northwest Europe (e.g. Sutton and Hodson, 2005). The strength of the westerly winds is strongly associated with the North Atlantic Oscillation (NAO), which is a dominant atmospheric pattern of climate variability over the North Atlantic (Hurrell et al. 2003).

Since 2004, the AMOC has been monitored by an array of moorings deployed along about 26.5°N (Cunningham et al. 2007; Johns et al. 2011; Rayner et al. 2011), supplemented by measurements of the Gulf Stream transport using submarine telephone cables in the Florida Straits (Baringer and Larsen, 2001) (Figure 1). It has been documented that changes in the AMOC can affect the sea level around the periphery of the North Atlantic (Levermann et al. 2005), in particular, along the U.S. east coast (Ezer et al. 2013; Yin and Goddard 2013; McCarthy et al. 2015; Little et al. 2017), although they are probably less important than the

directly wind-induced variability (Woodworth et al. 2014; Little et al. 2017). In 2009-2010, the AMOC temporarily slowed down by 30%, partially due to an extreme negative NAO, when the associated wind field reduced and (for some time) even reversed the northward Ekman transport component of the AMOC (McCarthy et al. 2012; Srokosz and Bryden 2015). It is possible that this slowdown of the AMOC and the wind anomalies led to an extreme sea level rise along the east coast of North America (Goddard et al. 2015; Andres et al. 2013). In addition, the reduced meridional heat transport caused an upper-ocean cooling in the subtropical Atlantic and warming in the tropics that may have helped push the atmospheric circulation into record-low NAO negative states in both winters of 2009-2010 and 2010-2011 (Cunningham et al. 2013; Bryden et al. 2014).

Interestingly, on month-to-month time scales, the AMOC transport is negatively correlated with nearly basin-wide variations of sea level in the Mediterranean Sea: a stronger/weaker AMOC is associated with a lower/higher sea level (Figures 2 and 3). In particular, the observed AMOC slowdown in 2009-2010 and then again in winter 2010-2011 coincided with the extreme non-seasonal (annual and semi-annual signals removed) sea level anomalies in the Mediterranean Sea reaching amplitudes of about 10 cm reported in earlier studies (Landerer and Volkov 2013; Volkov and Landerer 2015). These extreme short-term sea level fluctuations have amplitudes larger than approximately 6 cm of the global mean sea level rise over the last two decades (e.g. Cazenave et al. 2014), and pose a flood threat for coastal communities and infrastructure, as well as a challenge for their understanding and prediction.

As in any semi-enclosed sea, the Mediterranean Sea level is determined by the local freshwater balance, exchanges with connected basins, and the local variations of depth-

integrated seawater density (steric changes). It has been shown that the non-seasonal fluctuations of the Mediterranean Sea level are mainly due to mass exchanges through the Strait of Gibraltar, related to NAO-modulated winds over the strait and the adjacent Atlantic Ocean (Fukumori et al. 2007; Menemenlis et al. 2007; Landerer and Volkov 2013; Calafat et al. 2012; Tsimplis et al. 2013; Volkov and Landerer 2015). An out-of-phase relationship between the non-seasonal bottom pressure fluctuations in the Mediterranean Sea and in the midlatitude North Atlantic has been reported and attributed to large-scale wind stress curl variations and NAO (Piecuch and Ponte, 2014). A number of earlier studies have also highlighted the important role of the NAO-modulated sea level pressure, freshwater and buoyancy fluxes in driving the Mediterranean Sea level (e.g. Tsimplis and Josey 2001; Tsimplis and Rixen 2002; Tsimplis et al. 2005). While the role of NAO in the variability of circulation in the subtropical North Atlantic and the Mediterranean Sea level has been well documented (e.g. Tsimplis and Josey 2001; Tsimplis et al. 2008; Tsimplis and Shaw 2008; Volkov and Fu 2011; Tsimplis et al. 2013; Volkov and Landerer 2015), it is also possible that the large-scale ocean circulation in the North Atlantic can impact the Mediterranean Sea level through ocean-atmosphere feedbacks (e.g. Marshall et al. 2001).

The present study adds a novel element to the existing canon in that it reports on the correlation between the AMOC and the Mediterranean Sea level. Although the Mediterranean Sea is an integral part of the North Atlantic air-sea-land coupled climate system, the relationship between sea level in the Mediterranean and the AMOC transport at 26.5°N has not yet been established and explored. It is not clear why the two remote and probably not directly related processes are correlated. Are the AMOC and sea level in the Mediterranean simply forced by

the same processes, such as the NAO? Or does the AMOC provide a forcing that directly and/or indirectly affects sea level in the Mediterranean? In this study, we use satellite altimetry observations of sea surface height, measurements of the meridional transports across 26.5°N, temperature and salinity fields and profiles, and an atmospheric reanalysis to reveal and document the dynamical mechanisms that linked the AMOC and the Mediterranean Sea level in 2004-2017.

The manuscript is organized as follows. In sections 2 and 3, we describe the data used in this work and data analysis methods, respectively. Section 4 reports on the observed correlations between the AMOC transport components, the Mediterranean Sea level, and the NAO. In sections 5 and 6, we explore the dynamical mechanisms responsible for the observed correlations. Finally, section 7 provides summary and discussion.

2. Data

2.2. Sea level measurements

For sea level, we used both the regional (Mediterranean Sea) and global monthly maps of sea level anomalies (SLA) for the time period from January 1993 to February 2017, processed and distributed by the Copernicus Marine and Environment Monitoring Service (CMEMS, http://marine.copernicus.eu/). The SLA maps are generated by merging measurements by up to four altimetry satellites, using all missions available at a given time. Prior to mapping, the along-track altimetry records are routinely corrected for instrumental noise, orbit determination error, atmospheric refraction, sea state bias, static and dynamic atmospheric pressure effects, and tides (Pujol et al. 2016). The global mean sea level has been subtracted from the SLA time

series at each grid point to focus on local dynamic fluctuations not related to global changes. The area-weighted average time series, SLA_{MS}, represents the Mediterranean basin-wide SLA.

Satellite altimetry data was supplemented with monthly tide gauge measurements at Marseille from 1900 to 2010 and Trieste from 1927 to 2010, obtained from the Permanent Service for Mean Sea Level (www.psmsl.org). These are the longest records available in the Mediterranean, dating back to the end of the 19th century, but the records at Trieste prior to 1927 have substantial (multi-year) gaps. Shorter-term gaps at Marseille were either filled by linear interpolation prior to 1993 or by altimetry data after 1993. The tide gauge records were corrected for the inverted barometer (IB) effect given by $IB = (P_{ref} - P_a)/(\rho g)$, where P_a is the sea level pressure (SLP), and P_{ref} is the SLP averaged over the entire ocean, ρ is the seawater density, and g is gravity.

2.2. Observations of AMOC at 26.5°N

Monitoring the AMOC at 26.5°N has been carried out since 2004 under the auspices of the RAPID/MOCHA/WBTS (hereafter RAPID) program (Smeed et al. 2017). Key measurements are collected at the western and eastern boundaries of the Atlantic Ocean at 26.5°N and on either side of the mid-Atlantic Ridge. Due to the sloping boundaries, several moorings at different locations and depths on the slope are combined to form a single profile as described in McCarthy et al. (2015). The resulting time series of temperature and salinity profiles at the boundaries are used to derive dynamic height anomaly profiles, from which the mid-ocean meridional geostrophic transport is calculated.

An estimate of the AMOC transport (T_{AMOC}) is obtained as the sum of (i) the upper mid-ocean transport down to the deepest northward velocity at ~1100 m (T_{UMO}) (Johns et al. 2005),

(ii) the Florida Current transport (T_{FC}) obtained by measuring the voltage difference across the Florida Strait using submarine telephone cables (Baringer and Larsen 2001), and (iii) the near-surface meridional Ekman transport (T_{EK}) estimated using the zonal wind stress from the European Centre for Medium-Range Weather Forecasts (ECMWF) ERA-Interim reanalysis (McCarthy et al., 2015): $T_{AMOC} = T_{FC}+T_{EK}+T_{UMO}$. The lower limb of the overturning (deep southward flow) is represented by the sum of the Upper (1100-3000 m) and Lower (3000-5000 m) North Atlantic Deep Water (NADW) transports, so that $T_{AMOC} \approx -(T_{UNADW}+T_{LNADW})$ (Cunningham et al. 2007).

Here, we use both the 12-hourly time series of the meridional transports across 26.5°N and the 12-hourly vertical profiles of temperature and salinity near the eastern and western boundaries from April 2004 to February 2017 provided by RAPID. The meridional heat transport is derived from the RAPID observing system as described in Johns et al. (2011). Temperature and salinity profiles are used to compute dynamic height anomalies. Because most of the RAPID moorings have the shallowest measurements in the 100-200 dbar depth range, the dynamic height profiles were extended up to the surface using a cubic extrapolation (McCarthy et al. 2015). The time series of meridional transports and dynamic height anomalies were averaged monthly thus yielding 155 monthly estimates.

2.3. Temperature and salinity data

The monthly gridded temperature and salinity profiles from January 2004 to February 2017, produced by Japan Agency for Marine-Earth Science and Technology (JAMSTEC) from all available data including (and mostly) Argo (Hosoda et al. 2008), are used to compute the

contribution to sea level variability in the North Atlantic from changes in density (the steric component):

$$SLA_{st} = -\rho_0^{-1} \int_{-H}^{0} \rho'(T,S,z)\, dz, \quad (1),$$

where ρ' is an in-situ density anomaly with respect to the time-mean, ρ_0 = 1027.5 kg m^{-3}, T is temperature, S is salinity, z is depth, and H is the reference depth for the integration. Because we focus on the upper limb of overturning (upper 1100 m), the steric sea level anomalies were referenced to 1100 m depth. The steric sea level anomalies (SLA_{st}) can be approximately (because of nonlinearity of the equation of state) decomposed into the thermosteric (SLA_t) and halosteric (SLA_s) components:

$$SLA_{st} \approx SLA_t + SLA_s = -\rho_0^{-1} \left(\int_{-H}^{0} \rho'(T,\bar{S},z)\, dz + \int_{-H}^{0} \rho'(\bar{T},S,z)\, dz \right) \quad (2),$$

where the overbar indicates the time mean values.

2.4. Atmospheric and reanalysis data

To link the observed changes in the ocean to atmospheric forcing, we used the monthly mean fields of sea level pressure (SLP), net surface heat flux (Q_{net}), wind stress, 10-m wind speed, and sea surface temperature (SST) for 1979-2017 time period provided by the ECMWF's ERA-Interim reanalysis project (Dee et al. 2011). The long tide gauge records at Marseille and Trieste were compared to T_{EK} at 26.5°N estimated from the ECMWF's ERA-20C reanalysis over the 1900-2010 time interval (Poli et al., 2011). In addition, we used the monthly station-based NAO index, based on the difference of normalized SLP between Lisbon (Portugal) and Reykjavik (Iceland), and provided by the Climate Analysis Section of the National Center for Atmospheric Research (NCAR) (Hurrell, 2003).

3. Methods

The seasonal cycle was computed by fitting the annual and semi-annual harmonics in a least-squares sense and removed from all fields and time series. Wavelet coherence (Grinsted et al., 2004) is used to find regions in time-frequency space where SLA_{MS} and T_{EK} co-vary (Figure 4). Linear regression is used to examine the spatial patterns of SLP and wind changes with reference to the AMOC and Mediterranean Sea level variability: the monthly fields of SLP, zonal and meridional 10-m wind velocities are projected onto the monthly T_{AMOC} and SLA_{MS} time series (e.g. Figure 6). The corresponding regression coefficients are in Pa per Sv for T_{AMOC} and m s^{-1} per cm for SLA_{MS} (local changes in SLP and wind speed with respect to changes in the AMOC transport and Mediterranean Sea level, respectively).

To focus on the interannual variability, the monthly time series were further smoothed with a 'Lowess' filter with a 24-month span (approximately equivalent to a moving average with a 1-year window). An empirical orthogonal functions (EOF) analysis (von Storch and Zwiers, 1999) was used to identify the leading mode (EOF-1) of the interannual sea level variability in the North Atlantic (Figure 9). The spatial pattern of EOF-1 is represented as a regression map obtained by projecting the sea level data onto the standardized (divided by standard deviation) principal component (PC-1) time series. Thus, the regression coefficients are in centimeters (local change of sea level) per standard deviation change of PC-1.

The 95% significance level for correlation coefficients was estimated by computing correlations between the pairs of 10000 Monte Carlo simulations of random time series that have the same autocorrelation functions as the observed time series. For the non-seasonal monthly time series with 155 data points, the 95% significance level for correlation is about

194 0.2. For the smoothed time series (interannual signal), the 95% significance level for correlation
195 is about 0.5 at zero-lag and 0.6 at 12-month lag.

196 The net surface heat flux and temperature advection by ocean currents drive the
197 thermosteric sea level variability:

198 $$\frac{\partial SLA_t}{\partial t} = -\alpha\left(\frac{Q_{net}-\bar{Q}_{net}}{\rho_0 C_p} + \int_{-H}^{0} \mathbf{u}\cdot\boldsymbol{\nabla}T\,dz\right) \quad (3),$$

199 where α is the thermal expansion coefficient, C_p is the specific heat capacity of seawater, $\bar{Q}_{net}$ is
200 the climatological (averaged over 2004-2017) net surface heat flux (positive fluxes are directed
201 out of the ocean), and **u** is the ocean current velocity. We estimated the first term on the right
202 side of (3) using the ERA-Interim fields of Q_{net}. The spatially variable thermal expansion
203 coefficient was computed from the JAMSTEC fields of temperature and salinity and averaged
204 over the upper 100 m. The second (advection) term is largely unknown. However, by assuming
205 the ageostrophic component is well characterized by Ekman transport, the contribution of
206 temperature advection by Ekman transport can be approximated using a pseudo air-sea heat
207 flux following Marshall et al. (2001):

208 $$H_{Ek} = C_p\left(-\mathbf{k}\times\frac{\boldsymbol{\tau}}{f}\right)\cdot\boldsymbol{\nabla}SST \quad (4),$$

209 where **k** is the unit vector in the vertical, $\boldsymbol{\tau}$ is the wind stress, f is the Coriolis parameter, and
210 SST is the sea surface temperature, which is used as an approximation of the upper Ekman layer
211 temperature. For consistency with surface fluxes, we used the ERA-Interim wind stress and
212 SST. Then, assuming that the vertical heat advection is small, the thermosteric sea level change
213 of the upper 1100 m water column becomes

214 $$\frac{\partial SLA_t}{\partial t} \approx -\alpha\left(\frac{Q_{net}-\bar{Q}_{net}}{\rho_0 C_p} + \frac{H_{Ek}-\bar{H}_{Ek}}{\rho_0 C_p} + \int_{1100\,m}^{0} \mathbf{u}_{geos}\cdot\boldsymbol{\nabla}T\,dz\right) \quad (5),$$

where $\mathbf{u}_{geos}$ is the geostrophic velocity. In this study, we are able to directly estimate only the first two terms on the right side of equation (5).

4. Observed correlations

4.1. Monthly variability

Displayed in Figure 3a are the monthly time series of the non-seasonal SLA_{MS} and T_{AMOC} at 26.5°N. The zero-lag correlation between them is −0.4, which is significant at 95% confidence (Table 1). The weaker than average AMOC transport is associated with the higher than average SLA_{MS}. This is particularly valid for the extremely large anomalies in both the AMOC and SLA_{MS} observed in 2009-2010. A strong decrease of the AMOC from about 21 Sv in December 2008 to about 9 Sv in January 2010 and then again in Dec 2010 was accompanied by the record high sea level anomalies of above 8 cm in the Mediterranean Sea. This happened when the NAO index also became strongly negative (Figure 3b). Similar events associated with the negative NAO, but with smaller changes in T_{AMOC} and SLA_{MS}, were repeated in 2012 and 2013.

As already mentioned, the correlation between the Mediterranean Sea level and T_{AMOC} is nearly basin-wide across the Mediterranean, except for some interior regions (Figure 2). It appears that the correlation is significant mainly due to high inverse correlation between SLA_{MS} and Ekman transport at 26.5°N ($r = -0.52$) (Table 1): the positive (northward) anomalies of T_{EK} are associated with the negative anomalies of SLA_{MS} and vice versa. The variability of T_{EK} at 26.5°N is part of the large-scale variability in winds over the North Atlantic. This large-scale variability is modulated by the NAO, which explains the high correlation ($r = 0.77$) between the monthly T_{EK} and NAO indices (Table 1). Probably due to its connection with T_{EK}, the NAO

237 is significantly correlated with T_{AMOC} (r = 0.43), which for the longer time scales has been
238 reported earlier (e.g. Stepanov and Haines, 2014; Delworth and Zeng, 2016).

239 To investigate whether the observed relationship between SLA_{MS} and T_{EK} in 2004-2017
240 holds for prior periods, we compared (i) the satellite altimetry record of SLA_{MS} to T_{EK} from
241 ERA-Interim in 1993-2017, and (ii) the tide gauge records at Marseille (1900-2010) and Trieste
242 (1927-2010) to T_{EK} from ERA-20C (1900-2010). The correlation between the monthly time
243 series of SLA_{MS} and T_{EK} is −0.43 (Figure 4a). The wavelet coherence (Figure 4b) shows that
244 the relationship is non-stationary, but time and frequency dependent. The relationship between
245 SLA_{MS} and T_{EK} becomes stronger after 2005, when the time series co-vary at most frequencies.
246 The time series co-vary out-of-phase, which is demonstrated by the predominantly left-oriented
247 arrows. The correlation between the longer tide gauge records and T_{EK} (not shown) is −0.21 for
248 Marseille and −0.22 for Trieste, significant at 95% confidence. The reduction of correlation
249 coefficient is due to the longer time series (more degrees of freedom), limited representativeness
250 of Marseille and Trieste tide gauge records for the basin-averaged Mediterranean Sea level
251 (correlation between the tide gauge records and altimetry SLA_{MS} in 1993-2017 is 0.6 for
252 Marseille and 0.8 for Trieste), and also because the uncertainties in Ekman transport computed
253 from the ERA-20C reanalysis are larger for pre-satellite era (prior to 1979) than for satellite
254 era.

255 The other components of the AMOC, T_{FC} and T_{UMO}, are not correlated with SLA_{MS} (Table
256 1). Their correlation with T_{AMOC} is also smaller (0.44 and 0.42, respectively) than correlation
257 between T_{EK} and T_{AMOC} (0.57). Therefore, at non-seasonal month-to-month time scales, wind
258 stress appears to be the main driver of the AMOC variability at 26.5°N. We find that both

259 T_{UNADW} and T_{LNADW} are also significantly correlated with the AMOC (r = −0.50 and −0.89,
260 respectively) (Table 1), which is expected because the northward T_{AMOC} is compensated by the
261 total southward North Atlantic Deep Water transport. However, T_{UNADW} is not correlated with
262 SLA_{MS} (r = −0.01), whereas T_{LNADW} is positively correlated with SLA_{MS} (r = 0.46) (Table 1).
263 We recall that the mid-ocean meridional transports provided by RAPID include the
264 (unmeasured) compensating flow that ensures a net-zero meridional volume transport
265 (McCarthy et al. 2015). It appears that the correlation between T_{LNADW} and SLA_{MS} is primarily
266 due to this compensating transport. If the compensating transport is subtracted from T_{LNADW},
267 then the correlation between SLA_{MS} and T_{LNADW} becomes −0.21. Since the LNADW layer lies
268 just above the reference level (4820 dbar), then it is the most sensitive to changes in the
269 compensating transport and is strongly influenced by it, whereas farther up in the water column
270 there tends to be more cancellation between the shear-related transport changes and the
271 opposing barotropic changes. Although T_{LNADW} from RAPID contains the unmeasured
272 compensating transport, it is well-correlated with an independent estimate of T_{LNADW} derived
273 solely from satellite time-variable gravity measurements (Landerer et al., 2015), meaning that
274 the RAPID estimate is robust. Note that since a substantial part of the barotropic compensation
275 is balancing Ekman transport variations, there is also a relatively high correlation between T_{EK}
276 and T_{LNADW} (−0.59) (Frajka-Williams et al. 2016).

277 *4.2. Interannual variability*

278 It should be noted that removing interannual signals from the time series does not
279 significantly affect the observed correlations (Table 1), suggesting that the zero-lag
280 relationships are dominated by month-to-month fluctuations. However, in addition to these

month-to-month variations, there are lagged correlations between the interannual signals of SLA_{MS} and meridional transports at 26.5°N (Figure 5 and Table 2). The maximum correlation between T_{AMOC} and SLA_{MS} is −0.78, with SLA_{MS} lagging behind T_{AMOC} by 6 months (Figure 5b). It has been reported earlier that the Ekman component plays a dominant role in the AMOC variability on short time scales, and the geostrophic component, represented mainly by T_{UMO}, becomes more important on interannual time scales (e.g. Buckley and Marshall, 2016). On these interannual time scales, we find that T_{UMO} is highly correlated with the Mediterranean Sea level: the correlation between T_{UMO} and SLA_{MS} reaches a maximum of −0.79 when the latter lags behind the former by 12 months (Figure 5b). This relationship suggests that the Mediterranean Sea level may respond to baroclinic changes in the subtropical North Atlantic, and in the remainder of the manuscript we will try to unveil the mechanisms that link these two remote processes. The correlation between T_{EK} and SLA_{MS} on interannual time scales is also significant ($r = -0.79$) at one-month time lag, and it is mainly due to the large anomalies in 2010 and in 2012/2013 (Figure 5a).

5. Wind forcing as a common driver

We have demonstrated that the correlation between the monthly SLA_{MS} and AMOC is mainly due to the relationship between these quantities and the atmospheric forcing that is expressed through the local Ekman transport at 26.5°N and through the gyre-scale NAO. In order to reveal the atmospheric circulation patterns that contribute to the variability of the AMOC and SLA_{MS}, here we present the regression of the monthly ERA-interim SLP and 10-m wind velocity fields on the AMOC and on SLA_{MS} time series (seasonal cycles removed). It appears that both the AMOC and SLA_{MS} are related to similar dipole SLP patterns reminiscent

303 to NAO, with one pressure center located at mid-latitude (the Azores High) and the other at
304 high-latitude North Atlantic (the Icelandic Low) (Figure 6). This suggests that the AMOC and
305 SLA_{MS} are both driven, at least partially, by the same mode of the large-scale atmospheric
306 variability. It is interesting to note, however, that the subtropical lobe of the pattern in Figure
307 6b is centered more toward the eastern part of the ocean and over western Europe than in Figure
308 6a.

309 As expected, the spatial pattern of regression between SLP and AMOC (Figure 6a) is mostly
310 determined by regression between SLP and T_{EK} (not shown). An increase/decrease of SLP at
311 mid-latitudes (~40°N) is associated with a strengthening/weakening of the North Atlantic
312 westerly and trade winds. The stronger/weaker trade winds in the subtropics around 26.5°N
313 drive the northward/southward near-surface Ekman transport anomalies and, thus, directly
314 impact the AMOC. An increase/decrease of SLP by about 0.8 mbar around 40°N, 35°W is
315 associated with a 1 Sv increase/decrease in the AMOC transport. The other AMOC constituents
316 (T_{FC} and T_{UMO}) are not significantly related to SLP changes in the North Atlantic (not shown),
317 however, ultimately their variability is in part the result of how the ocean thermohaline structure
318 and circulation adjust to the varying atmospheric forcing.

319 The month-to-month variability of SLA_{MS} is mostly driven by winds over the Strait of
320 Gibraltar and just west of it (Landerer and Volkov, 2013). This is essentially a basin-wide
321 barotropic response to the along-strait wind-setup that forces water into or out of the
322 Mediterranean Sea until the zonal sea level pressure gradient balances the wind stress
323 (Fukumori et al. 2007; Menemenlis et al. 2007). Because these winds are part of the North
324 Atlantic large-scale atmospheric circulation, it is not surprising that SLA_{MS} is related to a NAO-

like dipole SLP and associated atmospheric circulation patterns (Figure 6b). An increase/decrease of SLP by about 1 mbar around 45°N, 15°W is associated with northeastward/southwestward wind anomalies along the northwest African coast and eastward/westward wind anomalies across the Strait of Gibraltar that force water to flow into/out of the Mediterranean Sea and, thus, raise/lower its level surface by about 1 cm.

It is instructive to explore the atmospheric SLP and circulation pattern during the observed record-high Mediterranean Sea level and record-low AMOC in 2009-2011 and in 2013 relative to the 1979-2015 SLP and wind climatology (Figure 7a). For this, we present a composite map of SLP and 10-m wind velocity for the periods when SLA_{MS} (shown in Figure 3a) is greater than 4 cm (Figure 7b). During these periods, the Greenland anticyclone strengthened and expanded, while the subtropical and subpolar SLP centers became weaker and shifted southward by about 10°. These changes were associated with a southward shift of westerly and trade winds. The westerly winds became more zonal and centered near the latitude of the Strait of Gibraltar (~35°N), which led to stronger westerly winds along the strait itself that pumped water into the Mediterranean Sea and raised its sea level. At the same time, the usually northward Ekman transport at 26.5°N (directed 90° to the right of the wind direction in the Northern Hemisphere) weakened to almost zero (it can occasionally reverse, as seen in Figure 4a) and, therefore, reduced the AMOC transport.

6. Dynamic connection with the large-scale North Atlantic circulation

6.1. Relation to sea level in the eastern North Atlantic

Using an ocean general circulation model, Calafat et al. (2012) showed that on decadal time scales sea level at the Atlantic side of Gibraltar is correlated with sea level along the northwest

coast of Africa. The authors suggested that the long-shore wind forcing drives the coastal sea level variability, which by the means of coastally-trapped waves propagates towards the Strait of Gibraltar and ultimately translates to basin-wide changes of sea level in the Mediterranean. Here, we utilize this concept to understand the mechanism that links the North Atlantic large-scale geostrophic circulation and the Mediterranean Sea level.

Displayed in Figure 8 are the correlation maps between the monthly (unsmoothed) SLA_{MS} and SLA (Figure 8a), and the monthly (unsmoothed) dynamic height at the eastern boundary from RAPID moorings and SLA (Figure 8b). Despite minor differences, the two maps exhibit similar patterns, probably related to large-scale baroclinic processes as suggested by the correlation with the dynamic height. The correlation pattern is also consistent with the gyre-scale atmospheric circulation. When there is a cyclonic circulation anomaly in the subtropical North Atlantic (similar to the pattern in Figure 6b, associated with a positive sea level anomaly in the Mediterranean) the upper-ocean Ekman transport anomaly near the eastern boundary is directed onshore and, therefore, it tends to reduce the coastal upwelling typical for this region, deepen the thermocline, and, thus, produce a positive steric sea level anomaly along the African coast. In addition, the anomaly pattern shown in Figure 6b causes an anticyclonic (negative) wind stress curl anomaly along the eastern part of the RAPID line at 26.5°N, which leads to additional Ekman pumping and higher dynamic height.

In agreement with Calafat et al. (2012), there is a band of high correlation along the northwest African coast towards the Strait of Gibraltar (Figure 8). The correlation between the dynamic height from RAPID moorings and local SLA is about 0.6. The shallowest RAPID mooring near the eastern boundary sits at 1000 m depth and about 50 kilometers offshore. High correlation between the dynamic height computed from the mooring data and coastal sea level

from altimetry (Figure 8b) suggests that the latter can be partially controlled by baroclinic processes in the deep ocean. The existence of coastally-trapped waves means that whenever the sea level becomes high at a certain location near the coast, it also becomes high further poleward due to propagation (Gill, 1982). If we consider the characteristic poleward propagation speed of about 2 cm s^{-1} (for the first baroclinic mode) (Smith, 1978), it takes about 8 days for the sea level signal to propagate from 26.5°N to the Strait of Gibraltar. This explains why at the time scales considered in this study, monthly sea level anomalies along the African coast and in the Mediterranean Sea appear to be synchronous. A rather broad area of significant positive correlation in the tropical North Atlantic indicates that the coastal sea level is coupled to the sea level over the deep ocean. Therefore, the Mediterranean Sea level is also linked to baroclinic changes in the North Atlantic that can be related to the upper-ocean geostrophic circulation.

6.2. Tri-pole mode of sea level variability in the North Atlantic

It appears that the correlation pattern in Figure 8 is related to the first mode of the interannual sea level variability, as illustrated by the first EOF of the low-pass filtered (with a cutoff period of 1 year) SLA (Figure 9a) and SLA_{st} (Figure 9b), explaining 41.8% and 42.6% of the variance, respectively. Because the mass contribution to the interannual sea level variability is apparently small, the two independent observing systems (satellite altimetry and Argo) show very similar spatial (Figure 9a and 9b) and temporal (Figure 9c) patterns. The EOF-1 manifests a tri-pole pattern of the large-scale interannual sea level variability: the mid-latitude band stretching from the Caribbean to Europe and associated with the Gulf Stream and the North Atlantic Current varies out-of-phase with both the equatorial-tropical band including the Mediterranean and the subpolar North Atlantic. The temporal evolution of EOF-1 is well

correlated (r=0.79) with SLA_{MS} in 2006-2015 (Figure 9c) meaning that at least during this time interval the basin-averaged sea level in the Mediterranean was part of the large-scale sea level variability in the North Atlantic.

Interestingly, the RAPID section at 26.5°N lies exactly across the boundary between the mid-latitude and equatorial-tropical bands of the tri-pole sea level variability pattern. The western part of the section is within the mid-latitude band, while the eastern part of the section crosses the northeastward extension of the equatorial-tropical band, meaning that there is a zonal sea level gradient associated with EOF-1. This provides a direct link to the AMOC, because the upper mid-ocean transport at 26.5°N (T_{UMO}) is related to the zonal difference in pressure and sea level between the eastern and western boundaries of the North Atlantic (e.g. Frajka-Williams, 2015). We recall that T_{UMO} and SLA_{MS}, which is characteristic for the eastern boundary sea level, are not in phase (Figure 5a), and on average there is a 12-month time lag (Figure 5b, Table 2). The periods of the low sea level at the eastern boundary in winters 2007-2008 and 2011-2012 were followed by strengthening of the southward upper mid-ocean transport. And then, as the southward T_{UMO} reached maximum values in 2009 and 2012, the sea level at the eastern boundary and in the Mediterranean was increasing until it reached peak values in 2010 and 2013 (Figures 4a and 8c).

The time-mean profiles of temperature (Figure 10a) and salinity (Figure 10c) averaged between 10°W-40°W provide a possible explanation of why the southward/northward anomalies of F_{UMO} and the AMOC are associated with increasing/decreasing sea level in the equatorial-tropical/mid-latitude bands. Both the temperature and salinity profiles display a downward dome-shaped structure centered at 30°-35°N and associated with the mid-latitude band. Because the meridional temperature and salinity gradients (contours in Figures 9a and

9c) south of the dome are predominantly positive, the time-mean T_{UMO} (southward) advects heat and salt from the mid-latitude band to the equatorial-tropical band. Hence, the southward/northward anomalies of T_{UMO} can lead to heat and salt convergence/divergence in the equatorial-tropical band. It has been shown earlier that this process drives the subsurface temperature variability in the tropical North Atlantic (Wang and Zhang, 2013).

It is instructive to compare the thermohaline structures in October 2008 and in October 2010, when the sea level in the equatorial-tropical band was at low and maximum values, respectively (Figure 9c). The differences of temperature (Figure 10b) and salinity (Figure 10d) between October 2010 and October 2008 clearly show the upper ocean cooling and freshening in the mid-latitude band, and warming and salinification in the equatorial-tropical band. The temperature/salinity increase exceeded 1°C/0.1 psu in the upper 100 m and 0.2°C/0.02 psu at a depth of 500 m. The maximum increase of temperature and salinity in the tropics was centered at 20°N. The fact that temperature and salinity changes are not limited to the mixed layer indicates an important role of geostrophic advection in driving these changes.

At 26.5°N, the upper mid-ocean transport is correlated with the meridional heat transport (compare Figures 4a and 8c) derived from the RAPID/MOCHA/WBTS observing system (Johns et al. 2011). Apparently, the interannual variability of the AMOC and associated meridional heat transport is linked to the tripole mode of sea level variability in the North Atlantic. The negative (southward) heat transport anomalies in 2009 and 2012 were followed by the positive anomalies of heat content and, therefore, steric sea level in the equatorial-tropical band (Figure 9c), consistent with Cunningham et al. (2013) and Bryden et al. (2014) analyses. This provides another evidence that a reduction of the AMOC, associated with the strengthening of the southward T_{UMO}, can lead to heat convergence in the equatorial-tropical

band and, consequently, rising sea levels along the northwest coast of Africa and ultimately in the Mediterranean Sea.

6.*3. Mechanisms driving the thermosteric sea level change in 2008-2010*

We have shown that the difference in the thermohaline structure between October 2010 and October 2008 appears to be mechanistically related to the meridional advection of heat and freshwater. Changes in the thermohaline structure are in turn linked to changes in the steric sea level. The sea level change from October 2008 to October 2010 (Figure 11a) was mostly accounted for by the steric sea level change (Figure 11b). The differences between Figures 10a and 10b are largely due to the differences in the spatial resolution and sampling of satellite altimetry and Argo measurements. The thermosteric component (Figure 11c) determines the sign of the steric sea level change, but it is partly offset by the halosteric sea level change (Figure 11d). In agreement with temperature and salinity profiles (Figures 9b and 9d), the maximum thermosteric and halosteric sea level change is centered at about 20°N and concentrated in the eastern part of the tropical North Atlantic. The maximum thermosteric sea level change near the eastern boundary exceeds 8 cm and about 50% of this change is compensated by the halosteric component.

Because the thermosteric component (Figure 12a, same as Figure 11c) determines the sign of the sea level change near the eastern boundary of the North Atlantic, we further analyze what mechanisms caused the thermosteric sea level change in the region. According to equation (3), the thermosteric sea level variability is driven by the net surface heat flux and heat advection by ocean currents. Between October 2008 and October 2010, the net surface heat flux anomaly was negative, i.e. warming the ocean and raising the thermosteric sea level, over about 10-15°

460 tropical band centered at about 20°N (Figure 12b). The magnitude of the thermosteric sea level
461 change due to the net surface heat flux was amplified in the eastern part of the basin and reached
462 about 2 cm, while the total thermosteric sea level change reached 6-8 cm. Clearly, the net
463 surface heat flux does not fully explain the observed thermosteric sea level change in the region
464 and, therefore, the remaining amount of heat had to be advected by ocean currents. It should be
465 noted that the thermosteric sea level change due to Q_{net} (in equations 3 and 5) is somewhat
466 sensitive to the period, over which the mean climatology ($\bar{Q}_{net}$) was computed. Nevertheless,
467 we found that using longer periods, e.g. 2000-2017 (satellite era) and 1979-2017 (including pre-
468 satellite era), does not impact the conclusions. Furthermore, when these periods are used, the
469 contribution of Q_{net} is even smaller compared to using the 2004-2017 climatology.

470 We are not able to directly calculate the contribution of heat advection due to the lack of
471 velocity data, but using a pseudo air-sea heat flux given by the equation (4), we can evaluate
472 the role of the near-surface advection by Ekman currents (Figure 12c). Over the ocean interior,
473 the contribution of Ekman advection to the thermosteric sea level change in 2008-2010 is fairly
474 small and hardly exceeds 1 cm in the tropics and mid-latitudes. However, in the vicinity of the
475 eastern boundary between 20°N and 26°N the Ekman advection becomes important and its
476 contribution increases up to 4 cm towards the African coast. This agrees with Calafat et al.
477 (2012), who demonstrated the important role of heat advection by Ekman currents in the coastal
478 sea level changes south of 25°N. Complementing to their result, we note that in 2008-2010 the
479 Ekman heat advection near the African coast was also accompanied by a larger-scale
480 geostrophic heat advection into the equatorial-tropical band of the North Atlantic, which was
481 also associated with the coastal sea level rise. This result appears to be not sensitive to the
482 climatology of H_{Ek}(equation 5).

The advection of heat by geostrophic currents (the last term in equation 5) in 2008-2010 can be estimated indirectly as the residual of the thermosteric sea level change (Figure 12a) after subtracting the contributions of the net surface heat flux (Figure 12b) and Ekman advection (Figure 12c). The uncertainty of this estimate is unknown, and it arises from the uncertainties in Argo and ERA-Interim data products. Keeping in mind the shortcomings of the residual calculation, it is interesting to note that the residual provides an illustration of the likely dominance of geostrophic advection in driving the heat convergence in the equatorial-tropical band of the North Atlantic during the time interval considered, consistent with Cunningham et al. (2013) and Bryden et al. (2014). The associated sea level rise just south of the RAPID line and between October 2008 and October 2010 ranges from 4 to above 8 cm, which is greater than the combined contribution of the air-sea heat exchange and Ekman advection. More detailed studies of this and similar events using ocean models that realistically simulate the AMOC will help to elucidate the potential role of geostrophic advection.

7. Summary and Discussion

We have documented that from 2004 through 2016 the nearly basin-wide non-seasonal Mediterranean Sea level measured by altimetry satellites is significantly correlated with the AMOC measured by the RAPID array at about 26.5°N (Figures 2 and 3a). A stronger/weaker AMOC is associated with a lower/higher sea level in the Mediterranean, which was particularly pronounced during the record largest basin-mean sea level anomalies in 2010-2011 and 2013. We have shown that on the monthly time scales this correlation is mainly due to the correlation between the Mediterranean Sea level and the northward Ekman transport at 26.5°N. The northward Ekman transport in the tropics is driven by trade winds that are part of the subtropical

505 cell of the NAO pattern. The other two components of the AMOC, Florida Current (T_{FC}) and
506 upper mid-ocean (T_{UMO}) transports, are not correlated with the Mediterranean Sea level on
507 monthly time scales (Table 1). Nevertheless, there is a significant lagged correlation between
508 the Mediterranean Sea level and T_{UMO} at 26.5°N on interannual (periods greater than 1 year)
509 time scales: the southward/northward anomalies of T_{UMO} are followed by higher/lower sea level
510 anomalies in the Mediterranean about one year later (Figure 5, Table 2). At the same time, the
511 maximum correlation between the Mediterranean Sea level and Ekman transport at 26.5°N on
512 interannual time scales ($r = -0.79$) is observed at a one-month time lag. These observations
513 suggest that wind forcing can be a common driver for both the Mediterranean Sea level and the
514 AMOC on monthly to interannual time scales, while the large-scale ocean circulation
515 represented by the AMOC can affect the Mediterranean Sea level on interannual time scales.
516 While the connection with the wind-forced Ekman component of the AMOC appears to be
517 straightforward, the impact of large-scale ocean circulation is indirect and more complex.

518 The identified mechanisms responsible for the teleconnection between the Mediterranean
519 Sea level and the AMOC are sketched in a simplified diagram in Figure 13. We have shown
520 that both the AMOC and the Mediterranean Sea level are related to similar gyre-scale
521 atmospheric sea level pressure (SLP) and circulation patterns intrinsic to the NAO di-pole
522 pattern (Figure 6). An increase/decrease of SLP in the center of the North Atlantic subtropical
523 gyre, associated with a positive/negative NAO phase (Figure 13 a/b), is linked with a
524 strengthening/weakening of westerly winds in the mid-latitudes and trade winds in the
525 subtropics and tropics. The trade winds drive northward/southward Ekman transport anomalies
526 that directly strengthen/weaken the AMOC. Because winds over and in the vicinity of the Strait
527 of Gibraltar are also part of the large-scale atmospheric circulation in the North Atlantic, the

above changes are associated with southwestward/northeastward wind anomalies along the northwest African coast and westward/eastward wind anomalies over the Strait of Gibraltar. According to previous studies, these winds are able to modify the sea level gradient along the strait and cause barotropic sea level fluctuations in the Mediterranean (Fukumori et al. 2007; Menemenlis et al. 2007; Calafat et al. 2012; Landerer and Volkov, 2013; Volkov and Landerer, 2015).

Using altimetry and Argo data, we have shown that the Mediterranean Sea level is well correlated at a zero-lag with sea level in the tropical band of the North Atlantic, in particular along the northwest African coast stretching towards Gibraltar (Figure 8) in agreement with a previous modelling study by Calafat et al. (2012). This means that the AMOC, which depends on the sea level gradient across the North Atlantic and, thus, on sea level at the eastern boundary, is also related to the Mediterranean Sea level. This relationship is due to the large-scale interannual sea level variability in the North Atlantic, the leading mode of which exhibits a tripole spatial pattern, with the mid-latitude band varying out-of-phase with the equatorial-tropical and subpolar bands (Figures 8a and 8b). The temporal evolution of the tri-pole mode is correlated with both the AMOC and the Mediterranean Sea level (Figure 9c).

Given the dominance of the thermosteric component in the North Atlantic sea level variability, the tri-pole mode mainly reflects the redistribution of heat. The meridional heat transport estimated at 26.5°N is a good indicator of heat exchange between the mid-latitude and the equatorial-tropical bands, because the RAPID/MOCHA/WBTS observational array lies just across the boundary between the two bands. The observed heat convergence in the equatorial-tropical band with peaks in 2010 and 2013 was largely driven by the meridional heat transport across 26.5°N. The southward anomalies of the AMOC about one year prior to these peaks,

551 which were mainly due to the increased southward upper mid-ocean transport, advected heat
552 from the North Atlantic subtropical gyre, characterized by the downward doming of isotherms
553 as opposed to the upward doming of isotherms in the equatorial-tropical band. The associated
554 warming and sea level rise in the equatorial-tropical band extended northeastward towards the
555 Strait of Gibraltar along the African coast, and ultimately induced basin-wide changes of sea
556 level in the Mediterranean.

557 During a positive/negative NAO state (Figure 13 a/b) the eastern boundary of the North
558 Atlantic is also exposed to a surface cooling/heating anomaly. Thus, up to 25-30% of the
559 thermosteric sea level rise near the eastern boundary between 20-25°N in 2008-2010 was
560 accounted for by a surface heating anomaly (compare Figures 11a and 11b). At the same time,
561 the anticyclonic/cyclonic wind anomaly favors offshore/onshore Ekman transport near the
562 eastern boundary that leads to a local heat divergence/convergence and strengthens/reduces the
563 usual for this region upwelling. We have shown, that in 2008-2010 the contribution of the
564 Ekman-induced heat advection reached up to 30% of the thermosteric sea level rise near the
565 African coast between 20-25°N (compare Figures 11a and 11c). As pointed out earlier, a
566 positive/negative NAO state is also associated with westward/eastward wind anomalies over
567 the Strait of Gibraltar that force water to flow out/in the Mediterranean and, therefore, can
568 amplify the remote influence of surface and lateral buoyancy fluxes in the eastern subtropical
569 North Atlantic. Interestingly, on interannual time scales, the amplitude of the Argo-derived
570 steric sea level near the eastern boundary is about twice less that the amplitude of the altimetry-
571 derived Mediterranean Sea level. This is possibly because buoyancy fluxes in the eastern North
572 Atlantic and winds over the Strait of Gibraltar have an equal contribution to the Mediterranean
573 Sea level and amplify the effect of each other.

It is noteworthy that an increase/decrease of sea level near the eastern boundary changes the zonal sea level gradient across the subtropical North Atlantic and, therefore, provides a negative feedback mechanism on the AMOC changes through a reduction/strengthening of the near-surface southward geostrophic transport, i.e. the southward T_{UMO}. The peaks of sea level in the equatorial-tropical band in 2010 and 2013 are associated with the northward anomalies of the meridional heat transport followed by the local heat divergence and lowering of sea level in 2011-2012 and in 2013-2015, respectively (Figure 9c). Such a feedback mechanism could be part of a North Atlantic self-oscillatory system.

As for any nonlinear coupled system, it is difficult to single out the process that provides the primary forcing (AMOC or atmospheric forcing in our case). As we have seen, the atmospheric forcing does directly impact the AMOC via the northward Ekman transport. However, it is necessary to note that the NAO-modulated changes in the atmospheric circulation, as reflected in the northward Ekman transport at 26.5°N, are not necessarily coherent with changes in the large-scale geostrophic circulation. This is because the former is driven by convergence/divergence of Ekman flow and, therefore, is proportional to wind stress curl and not to wind stress. For example, T_{EK} and T_{UMO} are not correlated in 2004-2007, but starting from 2008 changes in T_{EK} follow changes in T_{UMO} with about a 10-month time lag (Figure 5). Therefore, while it is very likely that the geostrophic part of the AMOC is wind forced (e.g. Zhao and Johns, 2014), it is not a simple response to the NAO, and the mechanisms schematized in Figure 13 are not necessarily coincident. It has been reported that a 30% reduction of the AMOC in 2008-2009 was the largest contributor to the observed cooling in the upper 2 km of the subtropical North Atlantic, which may have pushed the atmospheric circulation into an NAO negative state in 2009-2010 (Cunningham et al. 2013; Bryden et al.

2014). This illustrates a likely ocean-atmosphere feedback mechanism that may have ultimately affected the Mediterranean Sea as well.

The analysis presented in this manuscript is the first attempt to provide a comprehensive and physically consistent explanation for the observed teleconnection between the AMOC and the Mediterranean Sea level from 2004 to 2017. It should be noted, however, that while the proposed mechanism appears to be valid for this particular period, it may not hold at all times. Continued observations by the RAPID/MOCHA/WBTS array and dedicated modelling exercises are required to shed more light on the observed teleconnection.

Acknowledgements

This work was supported by the NASA Ocean Surface Topography Science Team program (via Grant Number NNX13AO73G) and by the National Oceanic and Atmospheric Administration (NOAA) Atlantic Oceanographic and Meteorological Laboratory, and it was carried out in part under the auspices of the Cooperative Institute of Marine and Atmospheric Studies (CIMAS) of the University of Miami and NOAA, cooperative agreement NA10OAR4320143. The satellite altimetry data are processed and distributed by the Copernicus Marine and Environment Monitoring Service (CMEMS, http://marine.copernicus.eu/). Data from the RAPID-MOC/MOCHA/WBTS MOC monitoring array are jointly funded by the U.K. Natural Environment Research Council, the National Science Foundation, and NOAA; the 12-hourly MOC data are made freely available at www.rapid.ac.uk/rapidmoc and www.rsmas.miami.edu/users/mocha. The 26.5°N MOC array and Argo Program are part of the Global Ocean Observing System. The Argo data were collected and made freely available by the International Argo Program and the national programs that contribute to it

(http://www.argo.ucsd.edu, http://argo.jcommops.org). The monthly station-based North Atlantic Oscillation (NAO) index was retrieved from https://climatedataguide.ucar.edu/climate-data/hurrell-north-atlantic-oscillation-nao-index-station-based. The authors thank Drs. Sang-Ki Lee and Chris Hughes, and an anonymous reviewer for useful comments and suggestions on the initial version of the manuscript.

References

Andres, M., G. G. Gawarkiewicz, and J. M. Toole (2013), Interannual sea level variability in the western North Atlantic: Regional forcing and remote response, Geophys. Res. Lett., 40, 5915–5919, doi: 10.1002/2013GL058013.

Atkinson, C. P., H.L. Bryden, J. J.-M. Hirschi, and T. Kanzow (2010), On the seasonal cycles and variability of Florida Straits, Ekman and Sverdrup transports at 26°N in the Atlantic Ocean, Ocean Sci., 6, 837-859, doi:10.5194/os-6-837-2010.

Baringer, M.O., and J.C. Larsen (2001), Sixteen years of Florida current transport at 27°N, Geophys. Res. Lett., 26(16), 3179-3182.

Baringer, M.O., and J.F. Price (1997), Mixing and spreading of the Mediterranean outflow, J. Phys. Oceanogr., 27, 1654–1677.

Bingham, R.J., and C.W. Hughes (2012), Local diagnostics to estimate density-induced sea level variations over topography and along coastlines, J. Geophys. Res., 117, C01013, doi: 10.1029/2011JC007276.

Bryden, H.L., B.A. King, G.D. McCarthy, and E.L. McDonagh (2014), Impact of a 30% reduction in Atlantic meridional overturning during 2009-2010, Ocean Sci., 10, 683-691, doi:10.5194/os-10-683-2014.

Calafat, F.M., D.P. Chambers, and M.N. Tsimplis (2012), Mechanisms of decadal sea level variability in the eastern North Atlantic and the Mediterranean Sea, J. Geophys. Res.-Oceans, 117, C09022, doi:10.1029/2012JC008285.

Cazenave, A., H.-B. Dieng, B. Meyssignac, K. von Schukmann, B. Decharme, and E. Berthier (2014), The rate of sea level rise, Nature Clim. Change, doi:10.1038/NCLIMATE2159.

646 Cunningham, S. A., C. D. Roberts, E. Frajka-Williams, W. E. Johns, W. Hobbs, M. D. Palmer,
647 D. Rayner, D. A. Smeed, and G. McCarthy (2013), Atlantic Meridional Overturning
648 Circulation slowdown cooled the subtropical ocean, Geophys. Res. Lett., 40, 6202–6207,
649 doi:10.1002/2013GL058464.

650 Cunningham, S.A. et al. (2007), Temporal variability of the Atlantic Meridional Overturning
651 Circulation at 26.5N, Science, 317, 935-938.

652 Dee, D.P. et al. (2011), The ERA-Interim reanalysis: con guration and performance of the data
653 assimilation system, Q. J. Royal Meteorol. Soc., 137, 553–597.

654 Delworth, T.L., and F. Zeng (2016), The impact of the North Atlantic Oscillation on climate
655 through its influence on the Atlantic Meridional Overturning Circulation, J. Clim., 29, 941-
656 962, doi:10.1175/JCLI-D-15-0396.1.

657 Ezer, T., L.P. Atkinson, W.B. Corlett, and J.L. Blanco (2013), Gulf Stream's induced sea level
658 rise and variability along the U.S. mid-Atlantic coast, J. Geophys. Res. Oceans, 118, 685-697,
659 doi:10.1002/jgrc.20091.

660 Frajka-Williams, E., Meinen, C. S., Johns, W. E., Smeed, D. A., Duchez, A., Lawrence, A. J.,
661 Cuthbertson, D. A., McCarthy, G. D., Bryden, H. L., Baringer, M. O., Moat, B. I., and Rayner,
662 D. (2016), Compensation between meridional flow components of the Atlantic MOC at
663 26° N, Ocean Sci., 12, 481-493, https://doi.org/10.5194/os-12-481-2016.

664 Frajka-Williams, E. (2015), Estimating the Atlantic MOC at 26N using satellite altimetry and
665 cable measurements, Geophys. Res. Lett., 42, 3458-3464, doi:10.1002/2015GL063220.

666 Fukumori, I., D. Menemenlis, and T. Lee (2007), A near-uniform basin-wide sea level
667 fluctuation of the Mediterranean Sea, J. Phys. Oceanogr., 37(2), 338–358.

668 Goddard, P.B., J. Yin, S.M. Griffies, and S. Zhang (2015), An extreme event of sea-level rise
669 along the Northeast coast of North America in 2009-2010, Nat. Commun. 6:6346,
670 doi:10.1038/ncomms7346.

671 Grinsted, A., J.C. Moore, and S. Jevrejeva (2004), Application of the cross wavelet transform
672 and wavelet coherence to geophysical time series, Nonlinear Processes in Geophysics, Vol.
673 11, pp. 561-566.

674 Hall, M.M., and H.L. Bryden (1982), Direct estimates and mechanisms of ocean heat transport,
675 Deep-Sea Res., 29, 339-359, doi:10.1016/0198-0149(82)90099-1.

676 Hosoda, S., T. Ohira, T. Nakamura (2008), A monthly mean dataset of global oceanic
677 temperature and salinity derived from Argo float observations, JAMSTEC Rep. Res. Dev.,
678 Vol. 8, 47-59.

679 Hurrell et al. (2003) in The North Atlantic Oscillation: Climate Significance and Environmental
680 Impact, Geophysical Monograph 134, American Geophysical Union.

681 Johns, W.E., M.O. Baringer, L.M. Beal, S.A. Cunningham, T. Kanzow, H.L. Bryden, J.J.M.
682 Hirschi, J. Marotzke, C.S. Meinen, B.Shaw, R. Curry (2011), Continuous, array-based
683 estimates of Atlantic Ocean heat transport at 26.5°N, J. Clim., 24, 2429-2449,
684 doi:10.1175/2010JCLI3997.1.

685 Johns W.E., T. Kanzow, and R. Zantopp (2005), Estimating ocean transports with dynamic
686 height moorings: An application in the Atlantic Deep Western Boundary Current at 26°N,
687 Deep Sea Research I, 52(8): 1542-1567, doi:10.1016/j.dsr.2005.02.002.

688 Landerer, F.W., D.N. Wiese, K. Bentel, C. Boening, and M.M. Watkins (2015), North Atlantic
689 meridional overturning circulation variations from GRACE ocean bottom pressure
690 anomalies, Geophys. Res. Lett., 42, 8114-8121, doi:10.1002/2015GL065730.

691 Landerer, F. W., and D. L. Volkov (2013), The anatomy of recent large sea level fluctuations
692 in the Mediterranean Sea, Geophys. Res. Lett., 40, doi:10.1002/grl.50140.

693 Levermann, A., A. Griesel, M. Hofmann, M. Montoya, S. Rahmstorf (2005), Dynamic sea level
694 changes following changes in the thermohaline circulation, Climate Dyn., 24, 347-354,
695 doi:10.1007/s00382-004-0505-y.

696 Le Traon, P.-Y., F. Nadal, N. Ducet (1998), An improved mapping method of multisatellite
697 altimeter data, J. Atmos. Oceanic Technol., 15, 522–534. doi:10.1175/1520-
698 0426(1998)015<0522:AIMMOM>2.0.CO;2.

699 Le Traon, P.-Y., Y. Faugère, F. Hernandez, J. Dorandeu, F. Mertz, M. Ablain (2003), Can we
700 merge GEOSAT follow-on with TOPEX/Poseidon and ERS-2 for an improved description
701 of the ocean circulation? J. Atmos. Oceanic Technol., 20, 889–895, doi:10.1175/1520-
702 0426(2003)020<0889:CWMGFW>2.0.CO;2.

703 Little, C.M., C.G. Piecuch, and R.M. Ponte (2017), On the relationship between the meridional
704 overturning circulation, alongshore wind stress, and United States East Coast sea level in the
705 Community Earth System Model Large Ensemble, J. Geophys. Res. Oceans, 122, 4554-4568,
706 doi:10.1002/2017JC012713.

707 McCarthy, G.D., D.A. Smeed, W.E. Johns, E. Frajka-Williams, B.I. Moat, D. Rayner, M.O.
708 Baringer, C.O. Meinen, J. Collins, H.L. Bryden (2015): Measuring the Atlantic Meridional

709 Overturning Circulation at 26ºN, Progr. Oceanogr., 130, 91-111,
710 doi:10.1016/jpocean.2014.10.006.

711 McCarthy, G.D., I.D. Haigh, J. J.-M. Hirschi, J.P. Grist, and D.A. Smeed (2015), Ocean impact
712 on decadal Atlantic climate variability revealed by sea-level observations, Nature, 521, 508-
713 512, doi:10.1038/nature14491.

714 McCarthy, G.D., E. Frajka-Williams,W. Johns, M.O. Baringer, C.S. Meinen, H.L. Bryden, D.
715 Rayner, A. Duche, C. Roberts, and S.A. Cunningham (2012), Observed interannual
716 variability of the Atlantic meridional overturning circulation at 26.5N, Geophys. Res. Lett.,
717 39, L19609, doi:10.1029/2012GL052933.

718 Menemenlis, D., I. Fukumori, and T. Lee (2007), Atlantic to Mediterranean sea level difference
719 driven by winds near Gibraltar strait, J. Phys. Oceangr., 37, 359, doi:10.1175/JPO3015.1.

720 Osborn, T.J. (2011), Winter 2009/2011 temperatures and a record-breaking North Atlantic
721 Oscillation index, Weather, 66, 19-21.

722 Piecuch, C.G., and R.M. Ponte (2014), Nonseasonal mass fluctuations in the midlatitude North
723 Atlantic Ocean, Geophys. Res. Lett., 41, 4261-4269, doi:10.1002/2014JL060248.

724 Poli, P., H. Hersbach, D. Tan, D. Dee, J.-N. Thepaut, A. Simmons, C. Peubey, P. Laloyaux, T.
725 Komori, P. Berrisford, R. Dragani, Y. Tremolet, E. Holm, M. Bonavita, L. Isaksen, and M.
726 Fisher (2013), The data assimilation system and initial performance evaluation of the ecmwf
727 pilot reanalysis of the 20th-century assimilating surface observations only (era-20c), Ecmwf
728 era report series, ECMWF, Shinfield Park, Reading, 14.

729 Smeed, D., G. McCarthy, D. Rayner, B.I. Moat, W.E. Johns, M.O. Baringer, C.S. Meinen
730 (2017), Atlantic meridional overturning circulation observed by the RAPID-MOCHA-WBTS

731 (RAPID-Meridional Overturning Circulation and Heatflux Array-Western Boundary Time
732 Series) array at 26N from 2004 to 2015, British Oceanographic Data Centre - Natural
733 Environment Research Council, UK. doi: 10.5285/5acfd143-1104-7b58-e053-
734 6c86abc0d94b.

735 Smith, R.L. (1978), Poleward propagating perturbations in currents and sea levels along the
736 Peru coast, J. Geophys. Res., 83, 6083-6092.

737 Srokosz, M., and H.L. Bryden (2015), Observing the Atlantic Meridional Overturning
738 Circulation yields a decade of inevitable surprises, Science 348, 1255575,
739 doi:10.1126/science.1255575.

740 Stepanov, V.N., and K. Haines (2014), Mechanisms of Atlantic Meridional Overturning
741 Circulation variability simulated by the NEMO model, Ocean Sci., 10, 645-656,
742 doi:10.5194/os-10-645-2014.

743 Sutton, R.T., and D.L.R. Hodson (2005), Atlantic Ocean forcing of North American and
744 European summer climate, Science, 309, 115-118, doi:10.1126/science.1109496.

745 Trenberth, K.E., and J.M. Caron (2001), Estimates of meridional atmosphere and ocean heat
746 transports, J. Clim., 14, 3433-3443, doi:10.1175/1520-0442(2001)014.

747 Tsimplis, M. N., F. M. Calafat, M. Marcos, G. Jordà, D. Gomis, L. Fenoglio-Marc, M. V.
748 Struglia, S. A. Josey, and D. P. Chambers (2013), The effect of the NAO on sea level and on
749 mass changes in the Mediterranean Sea, J. Geophys. Res.-Oceans, 118, 944-952,
750 doi:10.1002/jgrc.20078.

751 Tsimplis, M.N., M. Marcos, S. Somot, and B. Barnier (2008), Sea level forcing in the
752 Mediterranean Sea between 1960 and 2000, Global Planet. Change, 63(4), 325–332,
753 doi:10.1016/j.gloplacha.2008.07.004.

754 Tsimplis, M.N., E. Alvarez-Fanjul, D. Gomis, L. Fenoglio-Marc, and B. Perez (2005),
755 Mediterranean Sea level trends: atmospheric pressure and wind contribution, Geophys. Res.
756 Lett., 32, L20602, doi:10.1029/2005GL023867.

757 Tsimplis M.N., and M. Rixen (2002), Sea level in the Mediterranean Sea: the contribution of
758 temperature and salinity changes, Geophys. Res. Lett., Vol. 29, No. 23,
759 doi:10.1029/2002GL015870.

760 Tsimplis, M.N., and S. A. Josey (2001), Forcing of the Mediterranean Sea by atmospheric
761 oscillations over the North Atlantic, Geophys. Res. Lett., 28(5), 803–806.

762 Volkov, D.L., and F.W. Landerer (2015), Internal and external forcing of sea level variability
763 in the Black Sea, Clim. Dyn., doi:10.1007/s00382-015-2498-0.

764 Volkov, D.L., and L.-L. Fu (2011), Interannual variability of the Azores Current strength and
765 eddy energy in relation to atmospheric forcing, J. Geophys. Res.-Oceans, 116, C11011,
766 doi:10.1029/JC007271.

767 Volkov, D.L., and L.-L. Fu (2010), On the reasons for the formation and variability of the
768 Azores Current, J. Phys. Oceanogr., 40, 2197-2220, doi:10.1175/2010JPO4326.1.

769 Wang, C. and L. Zhang (2013), Multidecadal Ocean Temperature and Salinity Variability in
770 the Tropical North Atlantic: Linking with the AMO, AMOC, and Subtropical Cell. J. Climate,
771 26, 6137–6162, https://doi.org/10.1175/JCLI-D-12-00721.1.

772 Woodworth, P. L., M. Á. M. Maqueda, V. M. Roussenov, R. G. Williams, and C. W. Hughes
773 (2014), Mean sea-level variability along the northeast American Atlantic coast and the roles
774 of the wind and the overturning circulation, J. Geophys. Res.-Oceans, 119, 8916-8935,
775 doi:10.1002/2014JC010520.
776 Yin, J., and P.B. Goddard (2013), Oceanic control of sea level rise patterns along the East Coast
777 of the United States, Geophys. Res. Lett., 40, 5514-5520, doi:10.1002/2013GL057992.
778 Zhao, J., and W. Johns (2014), Wind-forced interannual variability of the Atlantic Meridional
779 Overturning Circulation at 26.5N, J. Geophys. Res., 119, 2403-2419,
780 doi:10.1002/2013JC009407.

781 **Table 1.** Correlation coefficients between the non-seasonal sea level averaged over the
782 Mediterranean (SLA_{MS}), monthly station-based NAO indices, and meridional transports across
783 26.5°N: the AMOC transport (T_{AMOC}), the Florida Current transport (T_{FC}), Ekman transport
784 (T_{EK}), upper mid-ocean transport (T_{UMO}), Upper North Atlantic Deep Water transport
785 (T_{UNADW}), Lower North Atlantic Deep Water transport (T_{LNADW}). Correlation coefficients
786 between the time series, from which interannual signals have been removed, are shown in
787 brackets. The 95% significance level for correlation is about 0.2.

	SLA_{MS}	T_{AMOC}	T_{FC}	T_{EK}	T_{UMO}	T_{UNADW}	T_{LNADW}
SLA_{MS}		-0.40 (-0.44)	-0.18 (-0.21)	-0.52 (-0.53)	0.04 (-0.02)	-0.01 (0.00)	0.46 (0.50)
T_{AMOC}			0.44 (0.44)	0.57 (0.54)	0.42 (0.51)	-0.50 (-0.48)	-0.89 (-0.91)
NAO	-0.48 (-0.48)	0.43 (0.39)	0.13 (0.12)	0.77 (0.78)	-0.15 (-0.15)	-0.12 (-0.09)	-0.42 (-0.39)

788

Table 2. Maximum lagged correlation coefficients and time lags between the low-pass filtered (interannual) Mediterranean Sea level (SLA_{MS}) and meridional transports across 26.5°N (as shown in Figure 5b): the AMOC transport (T_{AMOC}), Ekman transport (T_{EK}), and upper mid-ocean transport (T_{UMO}). The 95% significance level for correlation is 0.5 at zero lag and 0.6 at 12-month lag.

	SLA_{MS}	Lag (months)
T_{AMOC}	−0.78	6
T_{EK}	−0.79	1
T_{UMO}	−0.79	12

Figure Captions

Figure 1. Bottom topography (color) and schematic representation of the main oceanic flows comprising the meridional overturning circulation (arrows) in the North Atlantic: pink arrows show the upper-ocean flows and light blue arrows indicate the deep flows. The surface area A, over which the steric sea level budget in the ECCO2 model was analyzed, is bounded by red lines. The zonal magenta line indicates the 26.5°N MOC monitoring array (RAPID/MOCHA/WBTS). Abbreviations: MAR - Mid-Atlantic Ridge, NAC - North Atlantic Current.

Figure 2. Correlation between sea level in the Mediterranean Sea and the AMOC transport across 26.5°N (monthly unsmoothed values with seasonal cycles removed). The 95% significance level for correlation ($r=-0.25$) is shown by the red dotted contour.

Figure 3. (a) AMOC transport across 26.5°N (black curve) with measurement uncertainty (shaded band) and SLA (global mean sea level and seasonal cycle have been subtracted) averaged over the Mediterranean Sea (red curve). Note that the y-axis for the transport is reversed. The correlation between the AMOC and SLA time series is −0.4. (b) Monthly station-based NAO index.

Figure 4. (a) The monthly time series of SLA_{MS} from satellite altimetry and T_{EK} at 26.5°N computed from the ERA-Interim zonal wind stress, and (b) the wavelet coherence between the time series in (a). The direction of the arrows in the coherence plot corresponds to the phase lag on the unit circle, with the backward direction indicating an out-of-phase relationship. The cone

of influence in the coherence plot (white dashed curve) indicates where edge effects occur in the coherence data.

Figure 5. (a) The smoothed time series of SLA_{MS} (red) and the AMOC transport components: (black) T_{AMOC}, (dotted black) T_{FC}, (dashed black) T_{EK}, (blue) T_{UMO}. Note that the y-axis for the transport is reversed. (b) Cross-correlation functions of (black) SLA_{MS} and T_{AMOC}, (dotted black) SLA_{MS} and T_{EK}, (blue) SLA_{MS} and T_{UMO}. All the time series were detrended.

Figure 6. The regression maps of monthly sea level pressure (SLP) and 10-m wind velocity from ERA-Interim projected on (a) the AMOC transport across 26.5°N and (b) sea level in the Mediterranean Sea using zero lag (monthly unsmoothed values with seasonal cycles removed).

Figure 7. Sea level pressure (color) and 10-m wind velocity (arrows): (a) 1979-2017 mean climatology and (b) composite for the periods when $SLA_{MS} \geq 4$ cm over the Mediterranean Sea (see Figure 3a).

Figure 8. Correlation maps: (a) correlation between the monthly sea level averaged over the Mediterranean and satellite altimetry SLA in the North Atlantic, and (b) correlation between the monthly dynamic height from the eastern boundary moorings and satellite altimetry SLA in the North Atlantic. The 95% significance level is ±0.2; the positive (negative) significance level is shown by red (cyan) contours.

Figure 9. The first empirical mode of sea level variability: the spatial patterns of EOF-1 of (a) SLA from satellite altimetry and (b) SLA_{ST} from JAMSTEC data, and (c) the time evolution (principal component) of EOF-1 for SLA (blue) and SLA_{ST} (red). In (c), blue curve with circles

shows SLA_{ms} and red curve shows the meridional heat transport across 26.5°N (note that y-axis for heat transport is reversed). The vertical magenta lines in (c) mark October 2008 and October 2010, when sea level in the equatorial-tropical band was at a local minimum and the record-high maximum, respectively.

Figure 10. The JAMSTEC time-mean profiles of (a) temperature and (c) salinity (color) averaged between 10°W-40°W, with the meridional gradients (contours) of temperature (°C per 100 km) and salinity (psu per 100 km) gradients, respectively. The differences of the low-pass filtered (b) temperature and (d) salinity profiles between Oct 2010 (high sea level near the eastern boundary) and Oct 2008 (low sea level near the eastern boundary).

Figure 11. Processes responsible for the sea level change from Oct. 2008 to Oct. 2010: (a) The total sea level change observed by satellite altimetry; (b) the steric sea level change derived from JAMSTEC gridded product; (c) the thermosteric sea level change; (d) the halosteric sea level change; e) the sea level change driven by the net surface heat flux; (f) the sea level change due to the Ekman temperature advection.

Figure 12. (a) Thermosteric sea level change from Oct. 2008 to Oct. 2010 (same as Fig. 10c) and processes responsible for this change: (b) the sea level change driven by the net surface heat flux; (c) the sea level change due to the Ekman temperature advection; and (d) the residual (d=a-b-c) illustrating the contribution of advection by geostrophic currents.

Figure 13. Sketch summarizing the physical mechanisms linking the AMOC at 26.5°N and sea level in the Mediterranean Sea. A positive/negative NAO phase is associated with a stronger/weaker than the average westerly and trade winds (subplot a/b). A

856 strengthening/weakening of the AMOC at 26.5°N on monthly and interannual time scales is
857 mainly due to both (i) the direct forcing by trade winds that drive the northward/southward
858 anomalies of Ekman transport and (ii) the baroclinic adjustment of the upper-ocean
859 thermohaline structure and circulation to variable atmospheric buoyancy and momentum
860 fluxes. Firstly, the AMOC and the Mediterranean Sea level are linked, because they are both
861 forced by the same NAO-induced atmospheric circulation pattern. Anticyclonic/cyclonic
862 anomalies of the subtropical atmospheric circulation drive the northward/southward Ekman
863 transport anomalies at 26.5°N, and they are associated with westward/eastward wind anomalies
864 over the Strait of Gibraltar that pump water out/in the Mediterranean Sea and, thus, lower/raise
865 its sea level. Secondly, on interannual time scales, a negative/positive anomaly of the
866 meridional heat transport leads to heat convergence/divergence in the equatorial-tropical band,
867 which is associated with sea level rise that affects the northwest coast of Africa and ultimately
868 the Mediterranean.

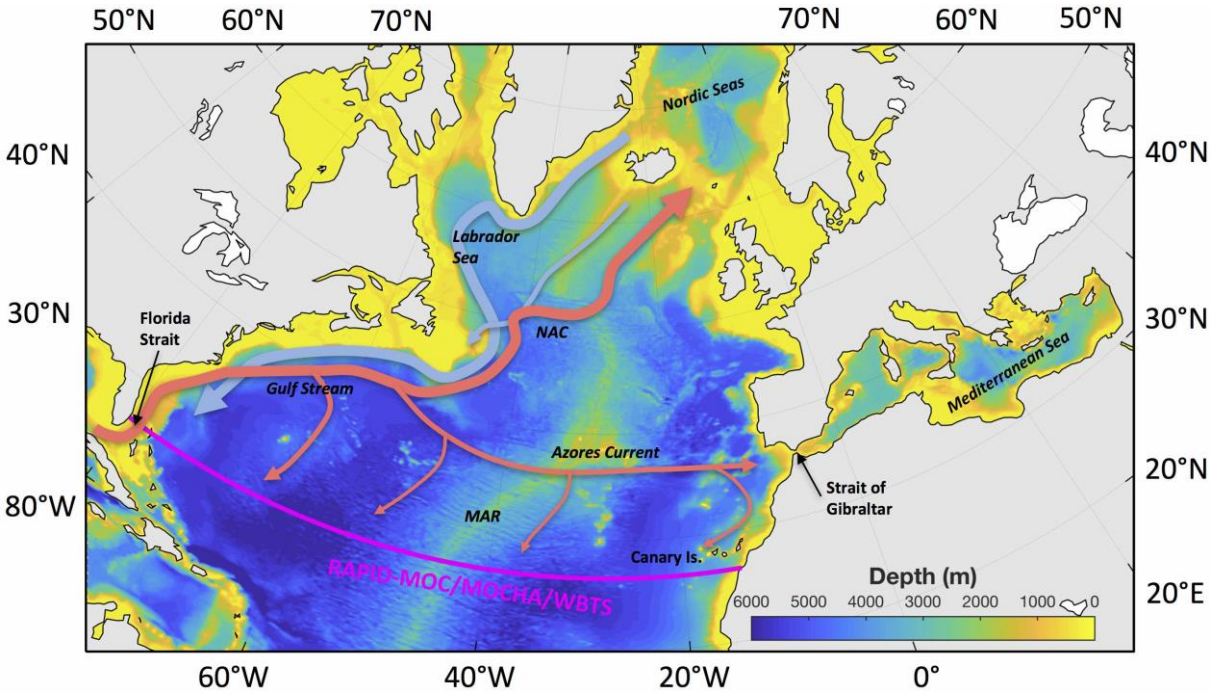

869

870 **Figure 1.** Bottom topography (color) and schematic representation of the main oceanic flows
871 comprising the meridional overturning circulation (arrows) in the North Atlantic: pink arrows
872 show the upper-ocean flows and light blue arrows indicate the deep flows. The surface area A,
873 over which the steric sea level budget in the ECCO2 model was analyzed, is bounded by red
874 lines. The zonal magenta line indicates the 26.5°N MOC monitoring array
875 (RAPID/MOCHA/WBTS). Abbreviations: MAR - Mid-Atlantic Ridge, NAC - North Atlantic
876 Current.

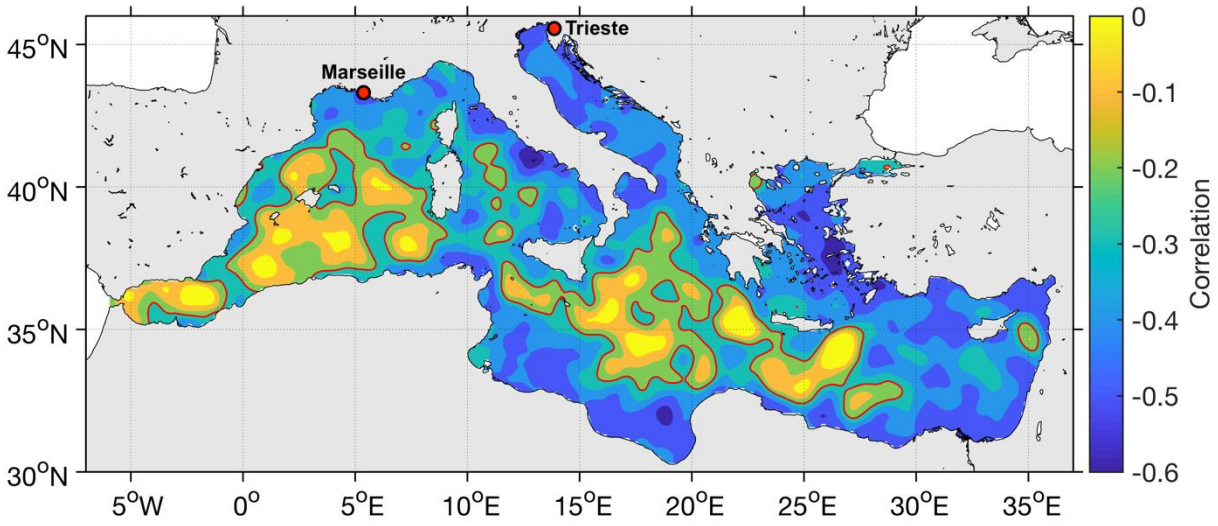

877

878 **Figure 2.** Correlation between sea level in the Mediterranean Sea and the AMOC transport
879 across 26.5°N (monthly unsmoothed values with seasonal cycles removed). The 95%
880 significance level for correlation ($r=-0.2$) is shown by the red contour. The locations of
881 Marseille and Trieste tide gauges are shown by red circles.

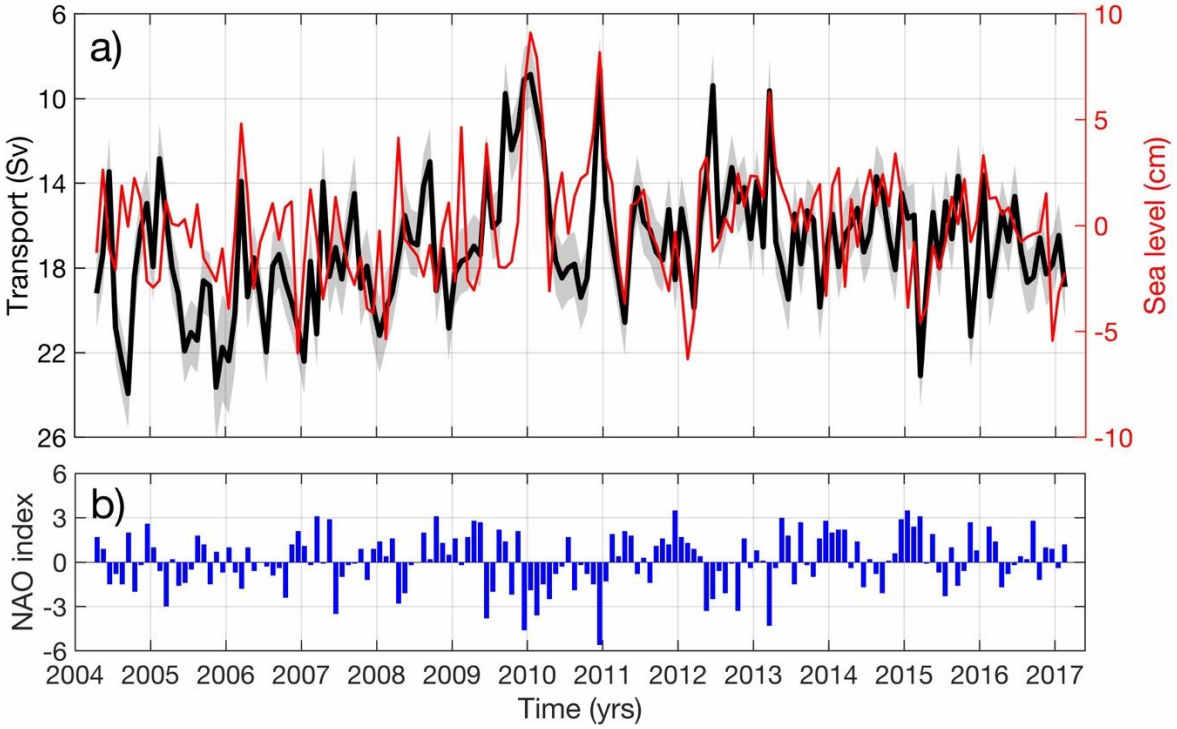

Figure 3. (a) AMOC transport across 26.5°N (black curve) with measurement uncertainty (shaded band) and SLA (global mean sea level and seasonal cycle have been subtracted) averaged over the Mediterranean Sea (red curve). Note that the y-axis for the transport is reversed. The correlation between the AMOC and SLA time series is −0.4. (b) Monthly station-based NAO index.

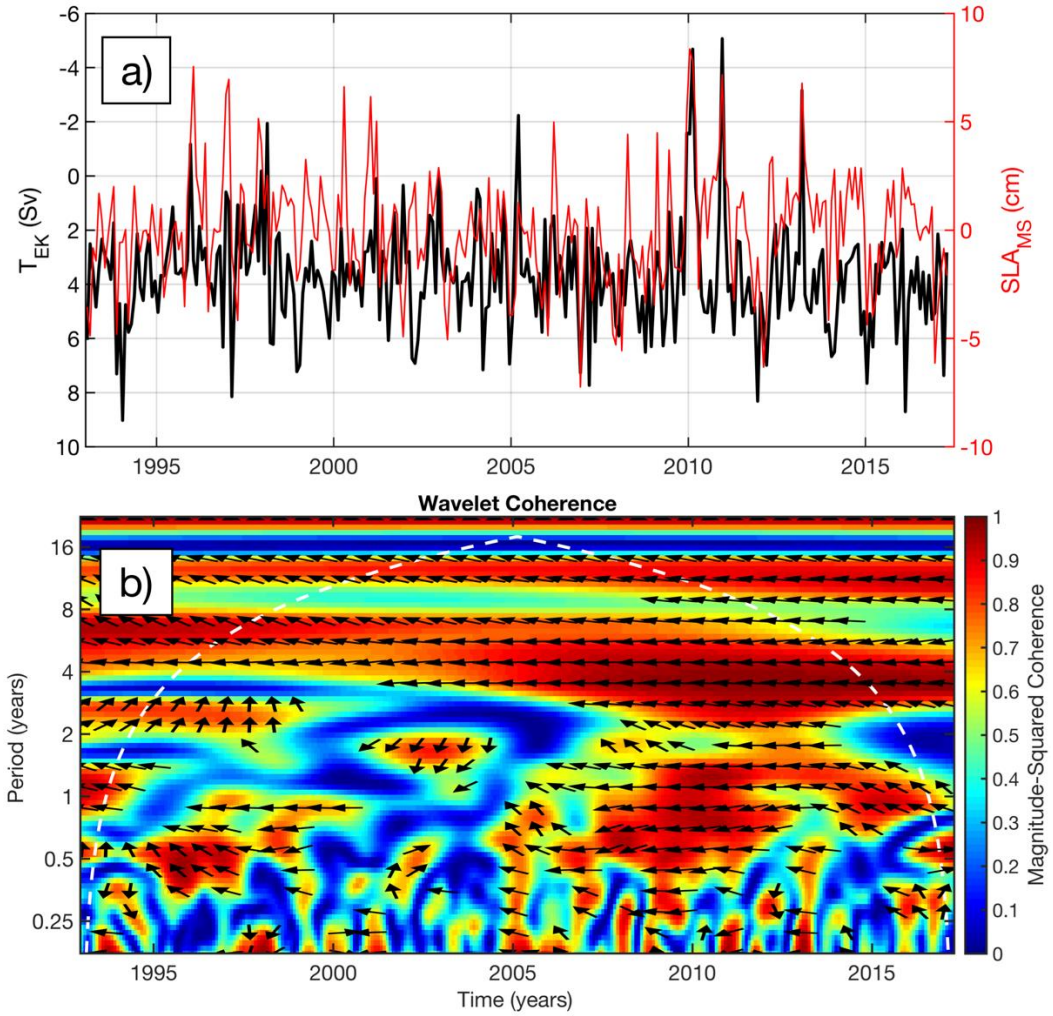

888

889 **Figure 4.** (a) The monthly time series of SLA_{MS} from satellite altimetry and T_{EK} at 26.5°N
890 computed from the ERA-Interim zonal wind stress, and (b) the wavelet coherence between the
891 time series in (a). Note that the y-axis for T_{EK} is reversed. The direction of the arrows in the
892 coherence plot corresponds to the phase lag on the unit circle, with the backward direction
893 indicating an out-of-phase relationship. The cone of influence in the coherence plot (white
894 dashed curve) indicates where edge effects occur in the coherence data.

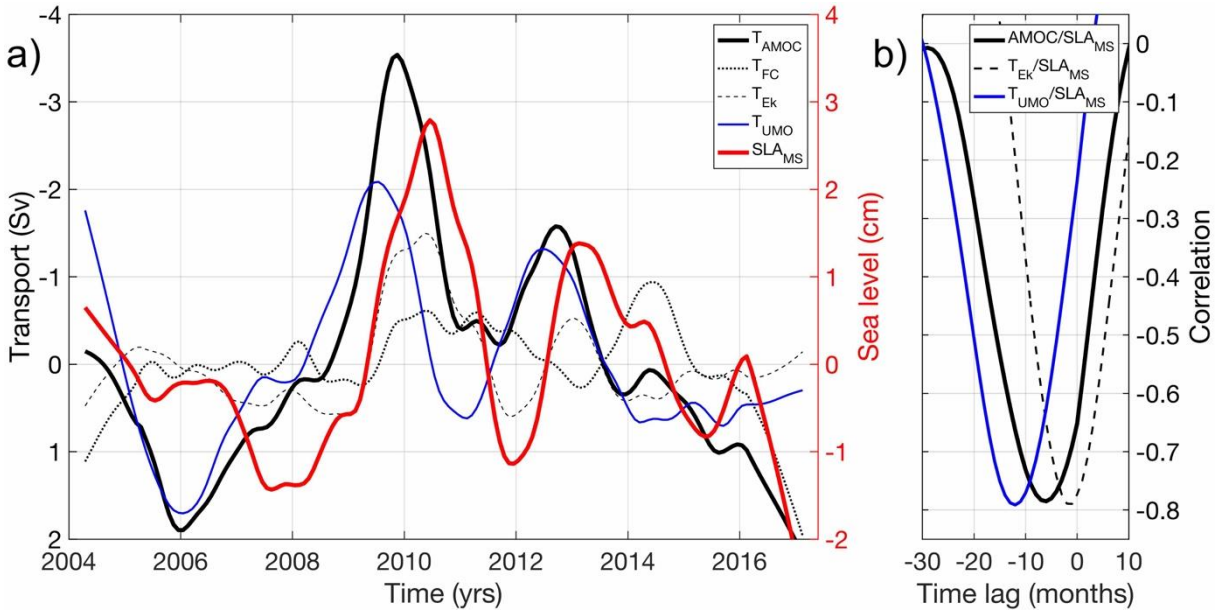

895

896 **Figure 5.** (a) The smoothed time series of SLA_{MS} (red) and the AMOC transport components:
897 (black) T_{AMOC}, (dotted black) T_{FC}, (dashed black) T_{EK}, (blue) T_{UMO}. Note that the y-axis for the
898 transport is reversed. (b) Cross-correlation functions of (black) SLA_{MS} and T_{AMOC}, (dotted
899 black) SLA_{MS} and T_{EK}, (blue) SLA_{MS} and T_{UMO}. All time series were detrended.

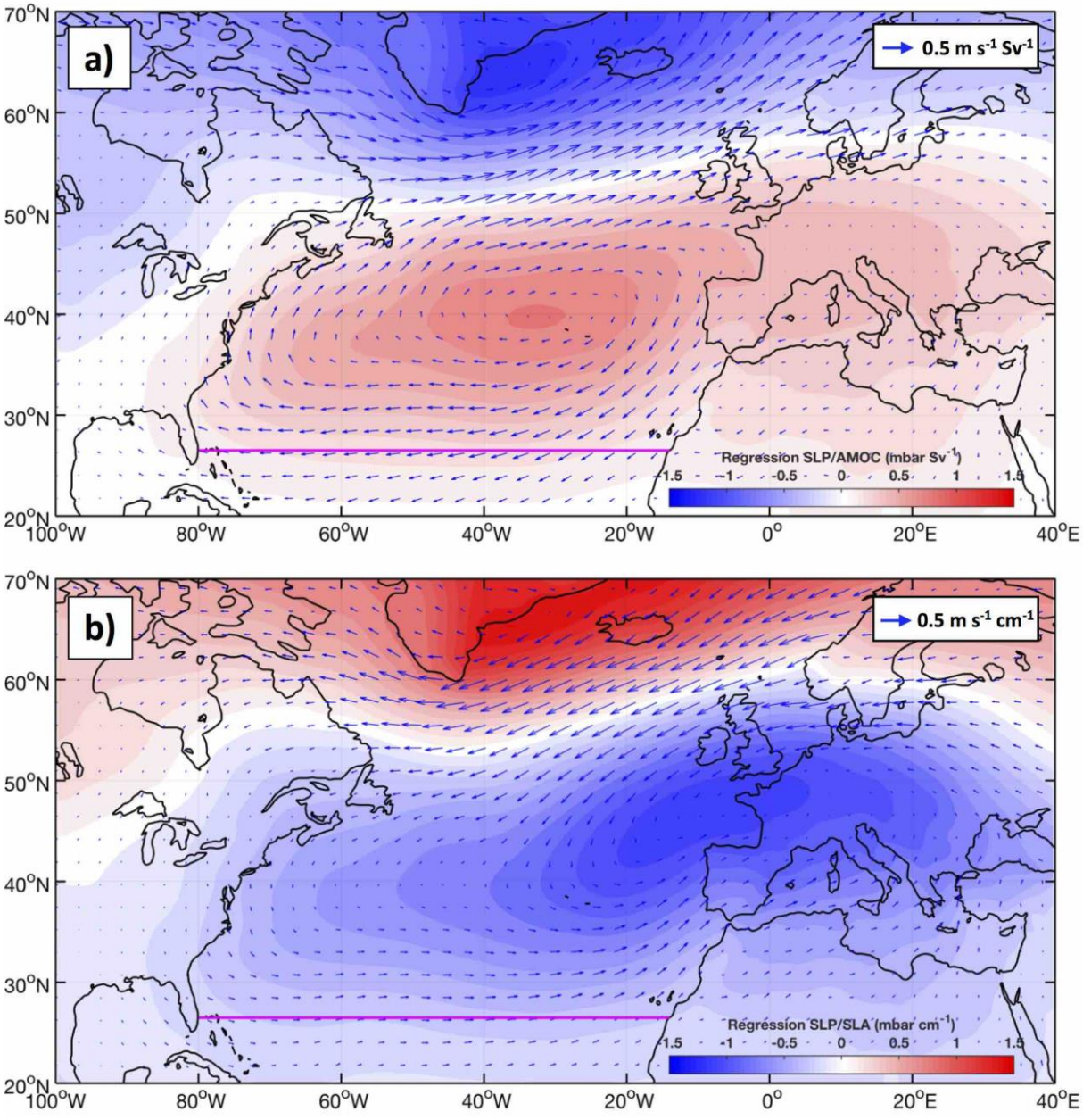

Figure 6. The regression maps of monthly sea level pressure (SLP) and 10-m wind velocity from ERA-Interim projected on (a) the AMOC transport across 26.5°N and (b) sea level in the Mediterranean Sea using zero lag (monthly unsmoothed values with seasonal cycles removed).

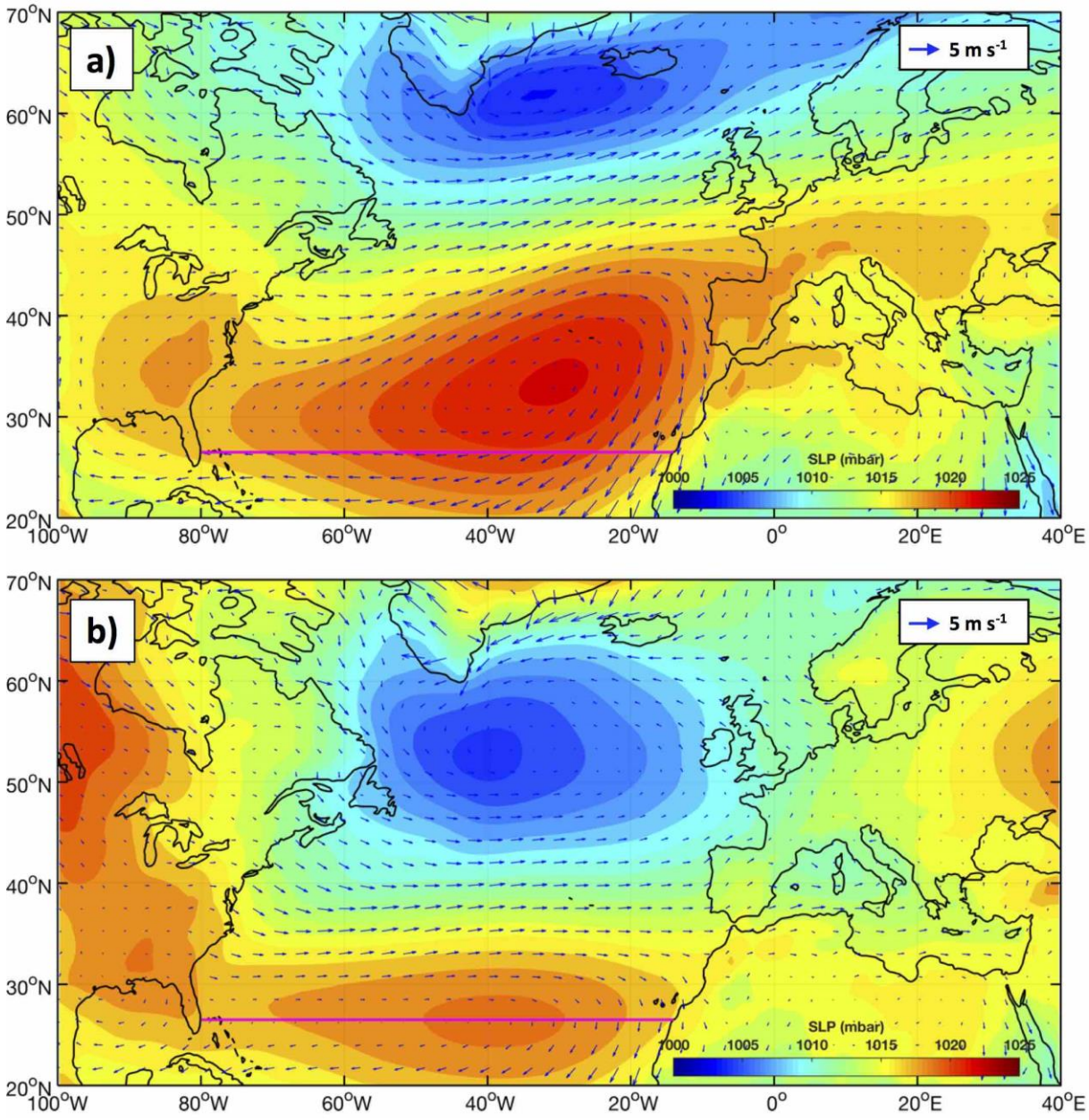

Figure 7. Sea level pressure (color) and 10-m wind velocity (arrows): (a) 1979-2017 mean climatology and (b) composite for the periods when $SLA_{MS} \geq 4$ cm over the Mediterranean Sea (see Figure 3a).

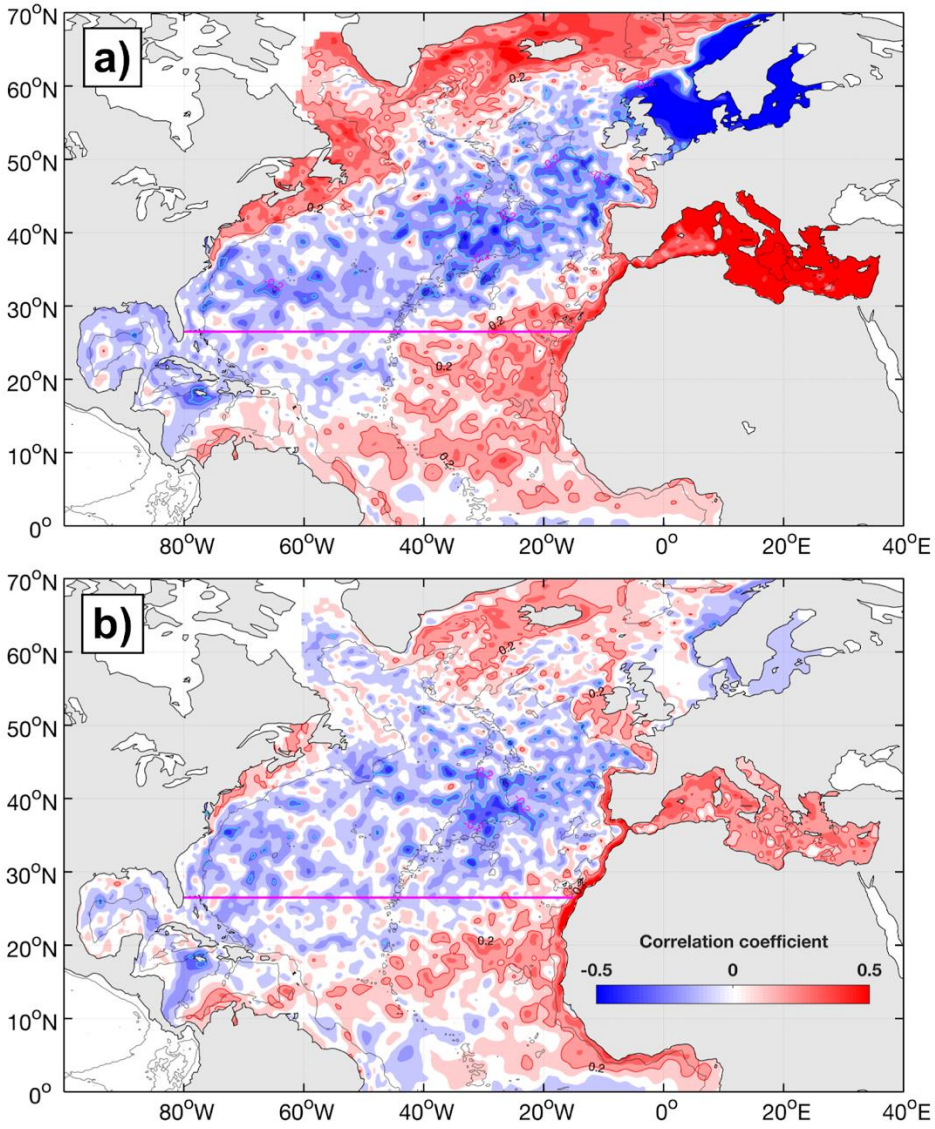

Figure 8. Correlation maps: (a) correlation between the monthly (unsmoothed) sea level averaged over the Mediterranean and satellite altimetry SLA in the North Atlantic, and (b) correlation between the monthly (unsmoothed) dynamic height from the eastern boundary moorings and satellite altimetry SLA in the North Atlantic. The 95% significance level is ±0.2; the positive (negative) significance level is shown by red (cyan) contours.

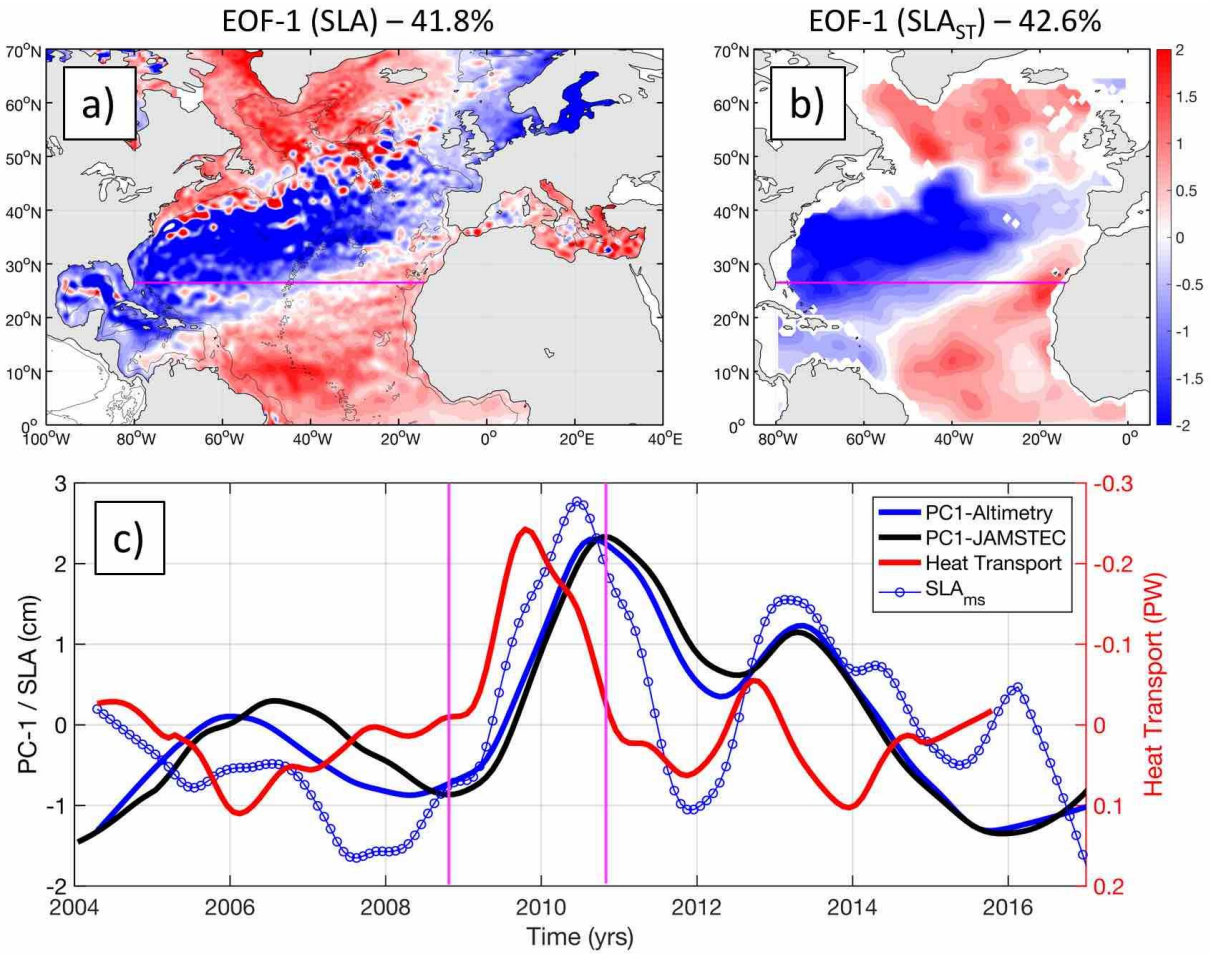

914

915 **Figure 9.** The first empirical mode of sea level variability: the spatial patterns of EOF-1 of (a)
916 SLA from satellite altimetry and (b) SLA_{ST} from JAMSTEC data, and (c) the time evolution
917 (principal component) of EOF-1 for SLA (blue) and SLA_{ST} (red). In (c), blue curve with circles
918 shows SLA_{ms} and red curve shows the meridional heat transport across 26.5°N (note that y-axis
919 for heat transport is reversed). The vertical magenta lines in (c) mark October 2008 and October
920 2010, when sea level in the equatorial-tropical band was at a local minimum and the record-
921 high maximum, respectively.

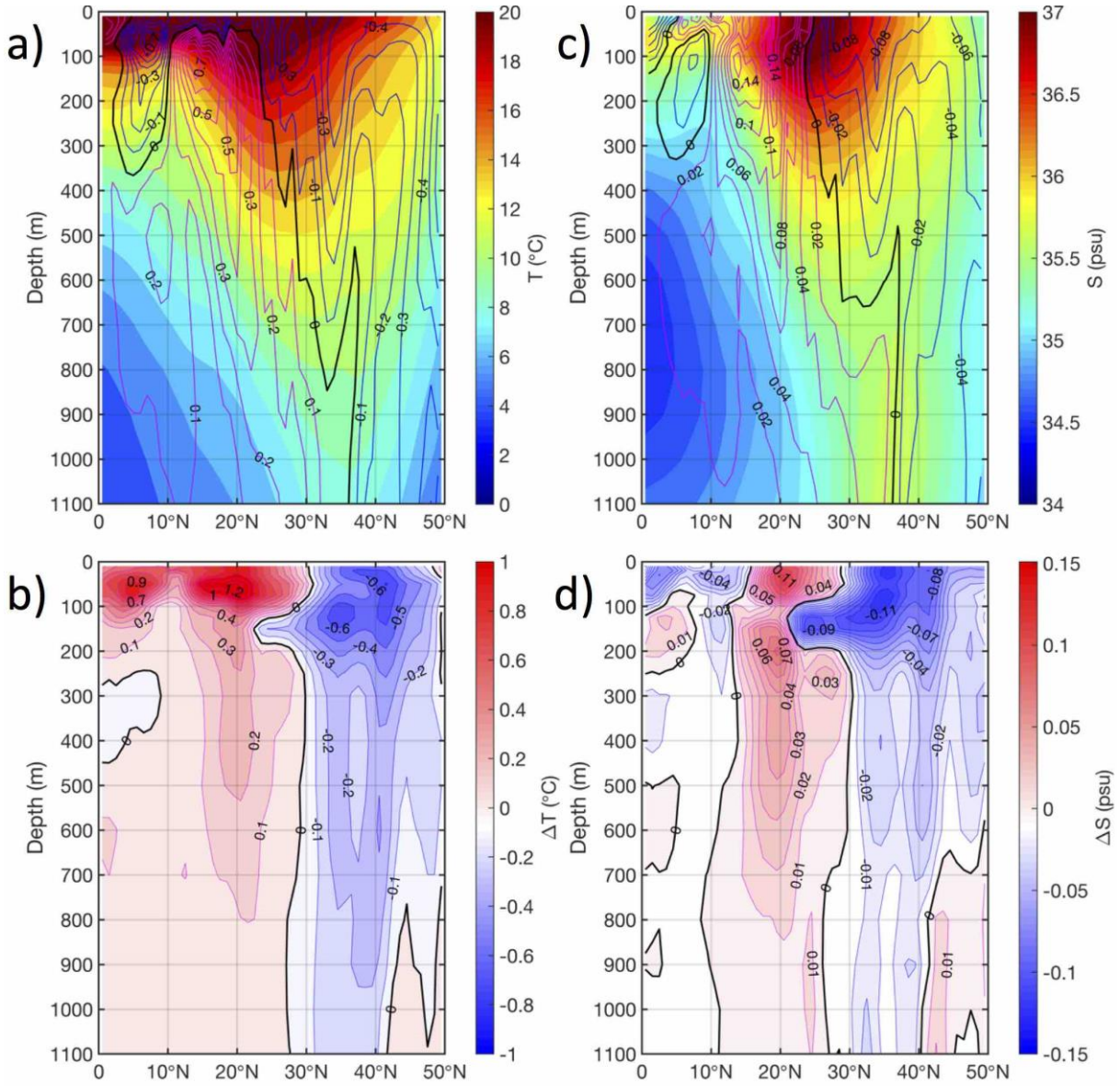

Figure 10. The JAMSTEC time-mean profiles of (a) temperature and (c) salinity (color) averaged between 10°W-40°W, with the meridional gradients (contours) of temperature (°C per 100 km) and salinity (psu per 100 km) gradients, respectively. The differences of the low-pass filtered (b) temperature and (d) salinity profiles between Oct 2010 (high sea level near the eastern boundary) and Oct 2008 (low sea level near the eastern boundary).

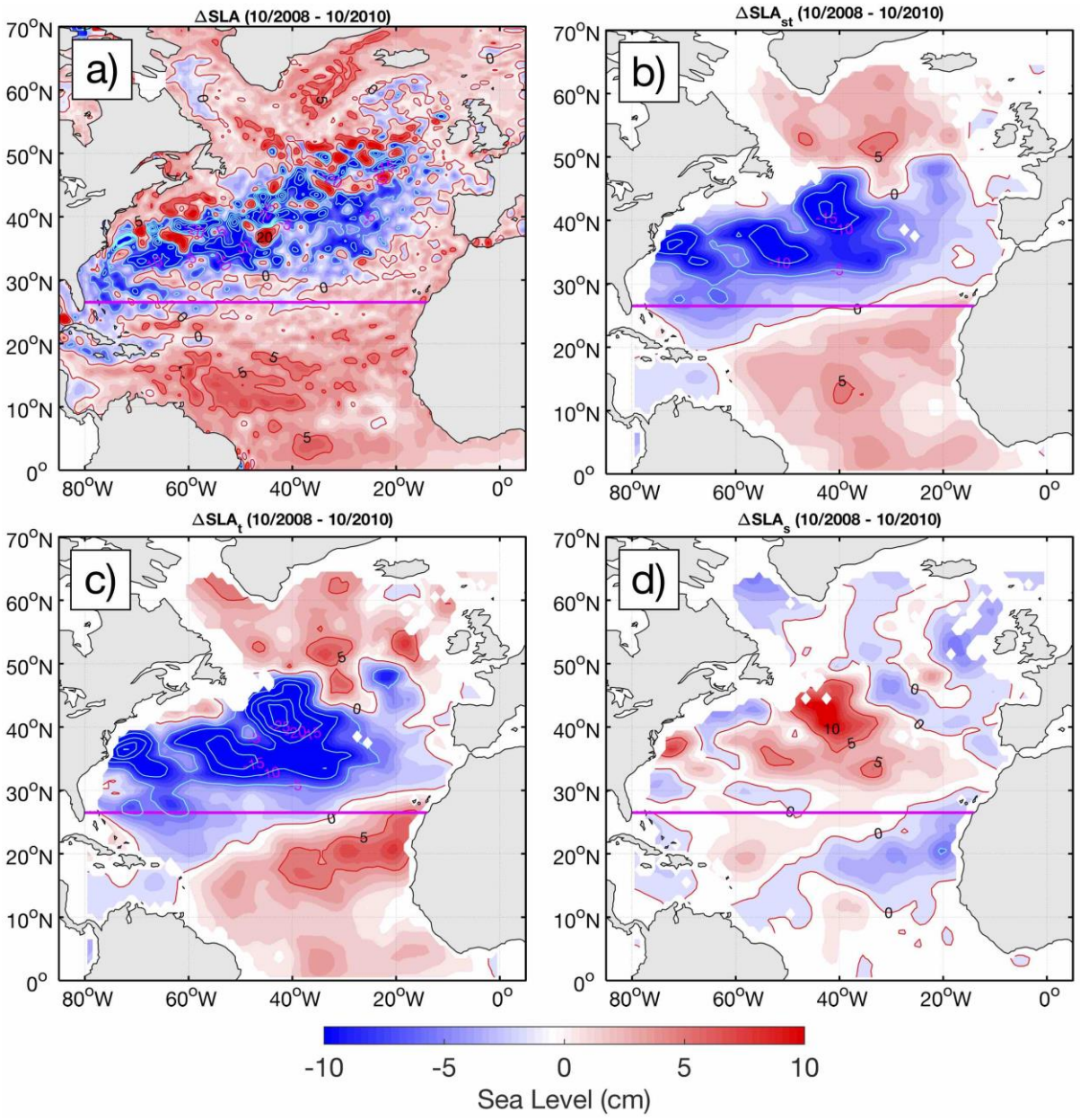

928

929 **Figure 11.** Processes responsible for the sea level change from Oct. 2008 to Oct. 2010: (a) The
930 total sea level change observed by satellite altimetry; (b) the steric sea level change derived
931 from JAMSTEC gridded product; (c) the thermosteric sea level change; (d) the halosteric sea
932 level change; e) the sea level change driven by the net surface heat flux; (f) the sea level change
933 due to the Ekman temperature advection.

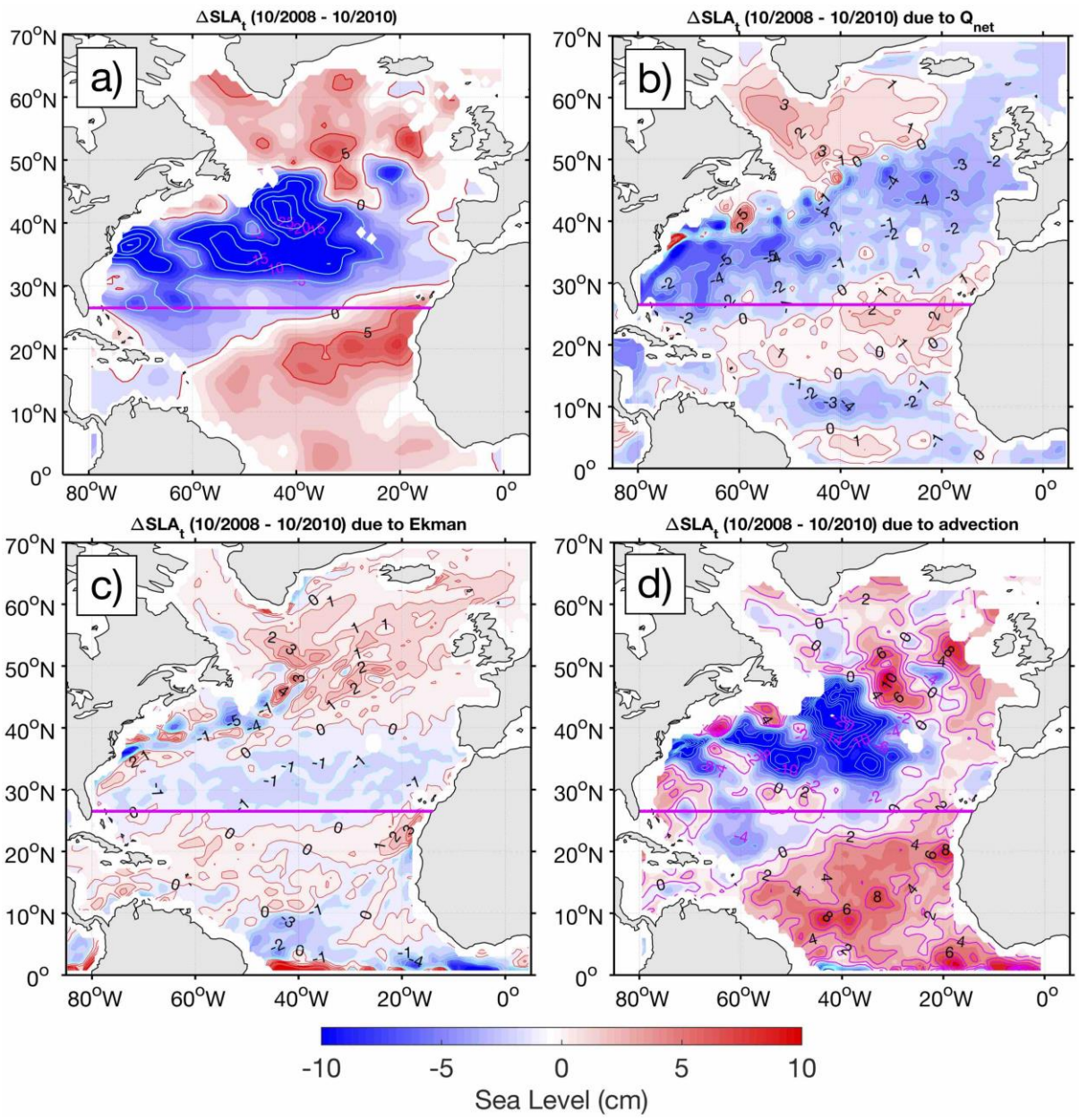

Figure 12. (a) Thermosteric sea level change from Oct. 2008 to Oct. 2010 (same as Fig. 10c) and processes responsible for this change: (b) the sea level change driven by the net surface heat flux; (c) the sea level change due to the Ekman temperature advection; and (d) the residual (d=a-b-c) illustrating the contribution of advection by geostrophic currents.

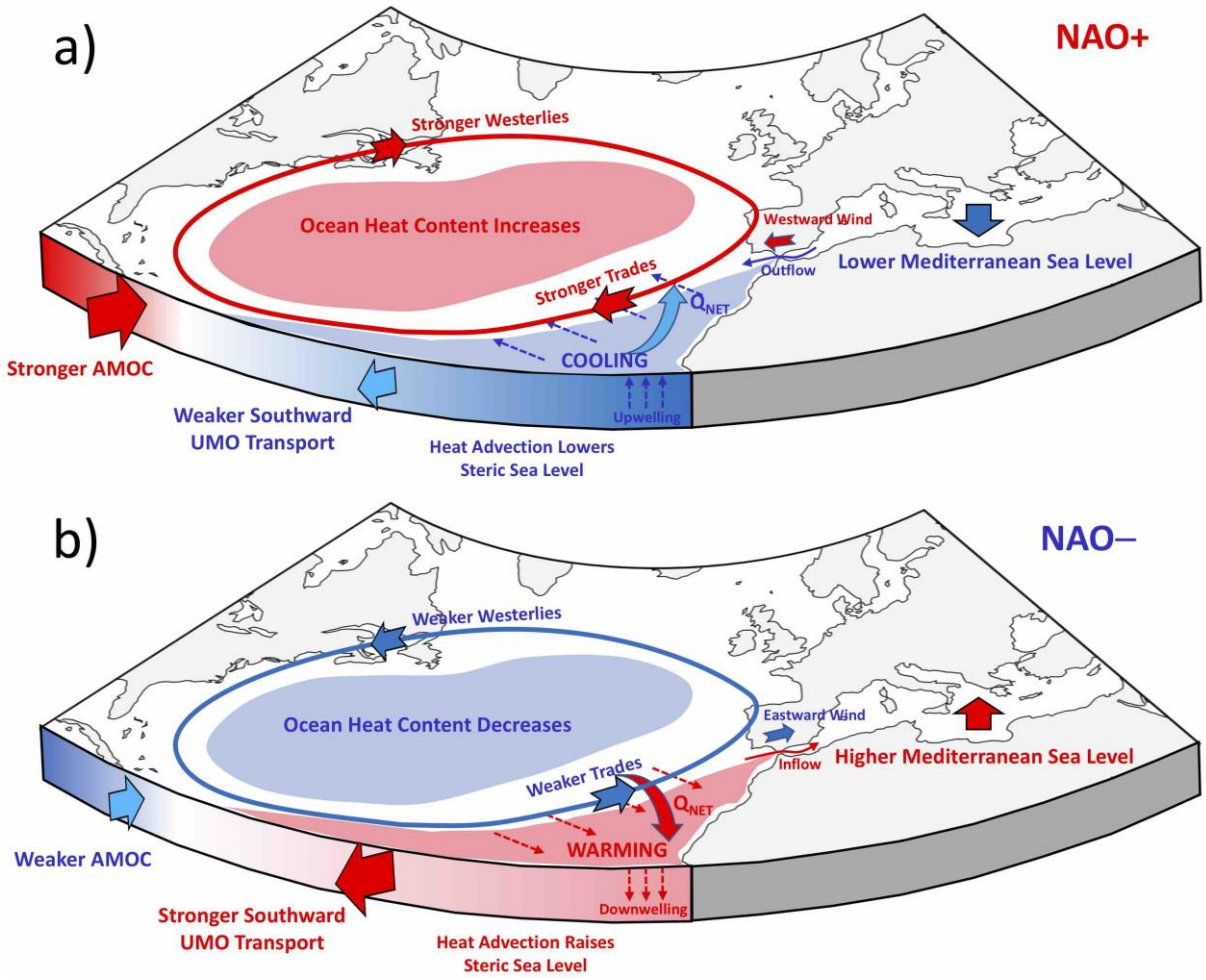

Figure 13. Sketch summarizing the physical mechanisms linking the AMOC at 26.5°N and sea level in the Mediterranean Sea. A positive/negative NAO phase is associated with a stronger/weaker than the average westerly and trade winds (subplot a/b). A strengthening/weakening of the AMOC at 26.5°N on monthly and interannual time scales is mainly due to both (i) the direct forcing by trade winds that drive the northward/southward anomalies of Ekman transport and (ii) the baroclinic adjustment of the upper-ocean thermohaline structure and circulation to variable atmospheric buoyancy and momentum fluxes. Firstly, the AMOC and the Mediterranean Sea level are linked, because they are both forced by the same NAO-induced atmospheric circulation pattern. Anticyclonic/cyclonic anomalies of the subtropical atmospheric circulation drive the northward/southward Ekman transport anomalies at 26.5°N, and they are associated with westward/eastward wind anomalies over the Strait of Gibraltar that pump water out/in the Mediterranean Sea and, thus, lower/raise its sea level. Secondly, on interannual time scales, a positive/negative anomaly of the meridional heat transport leads to heat divergence/convergence in the equatorial-tropical band, which is associated with sea level rise that affects the northwest coast of Africa and ultimately the Mediterranean.